Secretogranin III as a disease-associated ligand for antiangiogenic therapy of diabetic retinopathy

Michelle E. LeBlanc,[1] Weiwen Wang,[1] Xiuping Chen,[1,3] Nora B. Caberoy,[4] Feiye Guo,[1] Chen Shen,[1] Yanli Ji,[1,5] Hong Tian,[1,6,7] Hui Wang,[8] Rui Chen,[8] and Wei Li[1,2]

[1]Bascom Palmer Eye Institute and [2]Vascular Biology Institute, University of Miami School of Medicine, Miami, FL 33136
[3]Department of Ophthalmology, Zhongshan Hospital, Fudan University, Shanghai 200433, China
[4]School of Life Sciences, University of Nevada Las Vegas, Las Vegas, NV 89154
[5]Department of Ophthalmology, Zhengzhou Eye Hospital, Zhengzhou 450000, Henan, China
[6]School of Public Health, Xinxiang Medical University, Xinxiang, Henan 453003, China
[7]Everglades Biopharma, Miami, FL 33156
[8]Department of Molecular and Human Genetics, Baylor College of Medicine, Houston, TX 77030

Diabetic retinopathy (DR) is a leading cause of vision loss with retinal vascular leakage and/or neovascularization. Current antiangiogenic therapy against vascular endothelial growth factor (VEGF) has limited efficacy. In this study, we applied a new technology of comparative ligandomics to diabetic and control mice for the differential mapping of disease-related endothelial ligands. Secretogranin III (Scg3) was discovered as a novel disease-associated ligand with selective binding and angiogenic activity in diabetic but not healthy vessels. In contrast, VEGF bound to and induced angiogenesis in both diabetic and normal vasculature. Scg3 and VEGF signal through distinct receptor pathways. Importantly, Scg3-neutralizing antibodies alleviated retinal vascular leakage in diabetic mice with high efficacy. Furthermore, anti-Scg3 prevented retinal neovascularization in oxygen-induced retinopathy mice, a surrogate model for retinopathy of prematurity (ROP). ROP is the most common cause of vision impairment in children, with no approved drug therapy. These results suggest that Scg3 is a promising target for novel antiangiogenic therapy of DR and ROP.

INTRODUCTION

Diabetes afflicts ∼382 million people worldwide and may lead to diabetic vascular complications, such as coronary heart disease, atherosclerosis, diabetic nephropathy, diabetic neuropathy, and diabetic retinopathy (DR; van Dieren et al., 2010; Guariguata et al., 2014). DR affects ∼93 million people, including ∼28 million with vision-threatening diabetic macular edema (DME) and proliferative DR (PDR; Yau et al., 2012). DR in early stages is characterized by apoptosis of endothelial cells (ECs) and pericytes, vascular leakage, and leukocyte adhesion and may progress toward acellular capillaries, microaneurisms, retinal vein occlusion, DME, and PDR (Rask-Madsen and King, 2013). Angiogenic factors play an important role in the pathogenesis of DME with retinal vascular leakage and PDR with retinal neovascularization. A breakthrough in DME therapy is the advent and approval of vascular endothelial growth factor (VEGF) inhibitors ranibizumab (Lucentis) and aflibercept (Eylea; Schwartz et al., 2014). Compared with conventional laser photocoagulation therapy with relatively low efficacy, anti-VEGF therapy represents a remarkable advancement with improved efficacy (∼21–34%, vs. sham treatment; Nguyen et al., 2012; Virgili et al., 2014). However, the limited efficacy of VEGF inhibitors suggests that other angiogenic factors may also contribute to the pathogenesis of DR (Cerani et al., 2013). The challenge is how to identify other DR-related angiogenic ligands for alternative or combination therapy of anti-VEGF–resistant DME with high efficacy and safety. Additionally, there is no approved drug therapy for PDR without DME.

Similar to PDR, retinopathy of prematurity (ROP) with retinal neovascularization is the most common cause of vison loss in children, affecting ∼14,000–16,000 preterm infants each year in the US. ROP is currently treated with laser therapy or cryotherapy (Stahl et al., 2010). However, both treatments destroy the peripheral vision to save the central vision and do not address the underlying cause of ROP. Clinical trials revealed that VEGF inhibitors have limited efficacy for ROP (Mintz-Hittner et al., 2011). Given that VEGF is crucial to vascular and retinal development at embryonic and neonatal stages (Ferrara et al., 1996), clinical trial and off-label use of VEGF inhibitors for ROP therapy were associated with significant adverse outcomes (Lepore et al., 2014; Beharry et al., 2016). Thus, no drug therapy has been approved for ROP.

Correspondence to Wei Li: w.li@med.miami.edu

Abbreviations used: Cg, chromogranin; DME, diabetic macular edema; DR, diabetic retinopathy; EB, Evans blue; EC, endothelial cell; HDGF, hepatoma-derived growth factor; HRMVEC, human retinal microvascular EC; HRP-3, HDGF-related protein 3; MEK, mitogen-activated protein kinase; NGS, next generation DNA sequencing; OIR, oxygen-induced retinopathy; OPD, open reading frame phage display; pAb, polyclonal antibody; PDR, proliferative DR; ROP, retinopathy of prematurity; Scg, secretogranin; STZ, streptozotocin; VEGF, vascular endothelial growth factor; VEGFR, VEGF receptor.

The Rockefeller University Press $30.00
J. Exp. Med. 2017 Vol. 214 No. 4 1029–1047
https://doi.org/10.1084/jem.20161802

Secretogranin III (Scg3) belongs to the granin family, which consists of chromogranin A (CgA), CgB, and Scg2-7 (Taupenot et al., 2003). Scg3 is a binding partner of CgA and plays an important role in secretory granule biogenesis and peptide hormone secretion (Hosaka and Watanabe, 2010). Scg3 was reported to be secreted from dysfunctional β cells and, therefore, may be up-regulated in type 1 diabetes (Dowling et al., 2008). Scg3 is released from activated platelets in atherosclerotic lesions (Coppinger et al., 2004), which are one of the diabetic vascular complications (Rask-Madsen and King, 2013). One of the family members, Scg2, is a prohormone of secretoneurin with angiogenic activity (Kirchmair et al., 2004). Full-length CgA and its cleaved peptide vasostatin 1 ($CgA_{1–76}$) are potent angiogenesis inhibitors, whereas CgA-derived catestatin ($CgA_{352–372}$) is an angiogenic factor (Helle and Corti, 2015). However, Scg3 is the least studied member of the granin family and has not hitherto been reported as a cellular ligand or angiogenic factor.

In this study, we identified Scg3 as a disease-associated endothelial ligand in a mouse model of DR. We independently verified Scg3 as a highly disease-associated angiogenic factor and characterized its VEGF-independent signaling mechanisms. The pathogenic role and therapeutic potential of Scg3 were demonstrated by the capacity of its neutralizing antibodies to alleviate retinal vascular leakage and neovascularization in animal models of DR and ROP. Potential advantages for antiangiogenic therapy to target this disease-associated angiogenic factor are elaborated.

RESULTS

Quantitative ligandomic profiling

Cellular ligands, such as angiogenic factors, are traditionally identified by technically challenging, low-throughput approaches. It is even more daunting to delineate pathogenic ligands with therapeutic potential. To tackle the challenge, we developed open reading frame phage display (OPD) for the unbiased identification of cellular ligands in the absence of receptor information (Caberoy et al., 2010; Li, 2012). We further combined OPD with next generation DNA sequencing (NGS) as the first paradigm of ligandomics to globally map cell-wide endothelial ligands (LeBlanc et al., 2015). In this study, we applied comparative ligandomics analysis to diabetic and control mice to systematically identify disease-associated endothelial ligands and investigate their pathological role and therapeutic potential.

To establish DR in mice, we induced type 1 diabetes with streptozotocin (STZ), which destroys β islet cells (Zhong et al., 2012), and aged hyperglycemic mice for 4 mo to develop DR. As expected, we observed a 3.4-fold increase in retinal vascular leakage in diabetic mice (Fig. 1 F). For ligandomic analysis, we intravenously injected OPD libraries into diabetic and mock-treated control mice for three rounds of in vivo binding selection to enrich for retinal endothelial ligands (Fig. 1, A and G; LeBlanc et al., 2015). This selection was to enrich phage clones displaying ligands bound to their cognate receptors on the luminal membrane of ECs. All the cDNA inserts of enriched clones were analyzed by NGS. A total of 489,126 and 473,965 valid sequence reads were identified and aligned to 1,548 (diabetic retina) and 844 (healthy retina) proteins in the NCBI Consensus Coding Sequence (CCDS) database (Fig. 1 B; Fig. 2, A and B; Table 1; and Table S1). The identified ligands are involved in diverse cellular processes, ∼11.5% of which are related to angiogenesis, apoptosis, and cell migration and adhesion (Fig. 2 C).

We predicted that the copy numbers of cDNA inserts identified by NGS correlate with the endothelial binding activity of their cognate ligands. To confirm this correlation, we constructed two clonal phages expressing either human VEGF (hVEGF-Phage; positive control) or GFP (GFP-Phage; negative control). hVEGF-Phage displays wild-type human VEGF protein but with artificially altered codons for maximal silent mutations (Fig. S1) and can be distinguished from endogenous VEGF by NGS. Equal titers of hVEGF-Phage and GFP-Phage with nonmouse codons were diluted into the mouse OPD libraries (1:1,000) before in vivo selection and identified simultaneously within enriched library clones by NGS. The depletion of GFP-Phage and relative enrichment of hVEGF-Phage (GFP-Phage vs. hVEGF-Phage) after three rounds of selection confirmed that the copy numbers reflect their differential binding activities in vivo (Fig. 1 D and Table 1). Furthermore, the results established GFP-Phage as a baseline for nonspecific binding. We found that 417/844 and 817/1,548 isolated ligands specifically bound above this baseline to healthy and diabetic retina, respectively (Fig. 2, A and B).

Identification of Scg3 as a DR-high ligand by comparative ligandomics

The global binding activity patterns for the entire ligandome profiles of diabetic and healthy retinas were relatively similar (Fig. 2, A and B). However, more-detailed comparison revealed subtle differences for individual ligands. For example, Scg3 was detected with 1,731 copies in diabetic retina but zero copies in healthy retina (Fig. 1 D), implying that its receptors may be markedly up-regulated on diabetic endothelium. In contrast, the endothelial binding activity of hepatoma-derived growth factor (HDGF)–related protein 3 (HRP-3 or Hdgfrp3) to diabetic retina was reduced by 227-fold (Fig. 1 D), implicating that its receptors may be down-regulated in diabetes. VEGF binding activity was reduced only by 5.9-fold (Fig. 1 D), suggesting that retinal endothelial expression of VEGF receptors (VEGFRs) was minimally altered in 4-mo-old diabetic mice.

As a proof of concept for comparative ligandomics, we quantitatively compared the entire ligandome profiles for diabetic versus control retina by the χ^2 test. We identified 1,114 DR-associated endothelial ligands ($P < 0.05$) from a total of 1,772 nonredundant ligands (Fig. 1, C and E; and Fig. 2 D). We categorized them into DR-high and DR-low ligands based on their increased or decreased binding to diabetic ret-

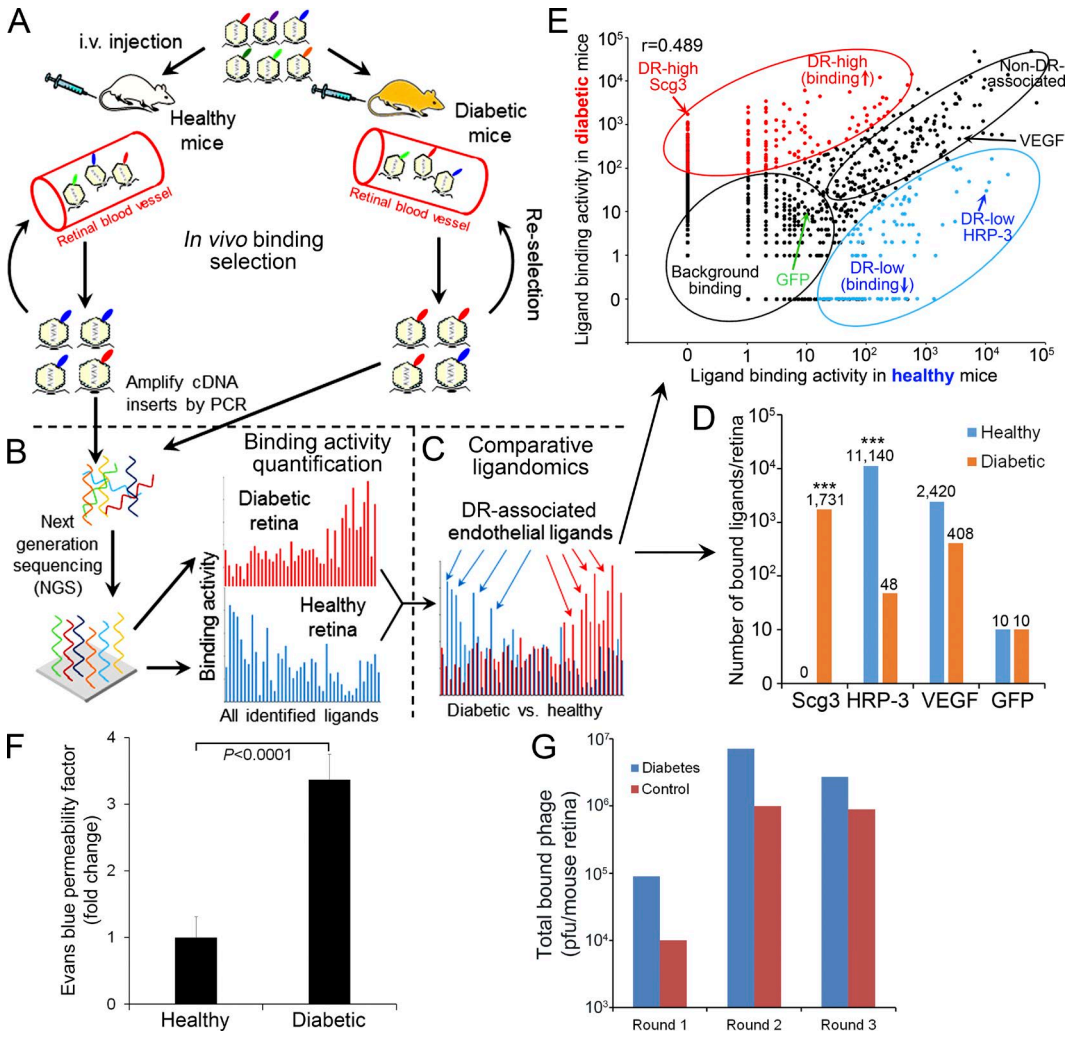

Figure 1. **Schematics of comparative ligandomics.** (A) Multi-round in vivo binding selection by OPD to enrich for retinal endothelial ligands in diabetic and healthy mice (see F). Three rounds of in vivo selection (three mice/round/group) were performed. Phage enrichment quantification is shown in G. (B) Global identification of all enriched ligands. After three rounds of selection, the cDNA inserts of enriched ligands were amplified by PCR and identified by NGS with simultaneous binding activity quantification for all identified ligands. (C) Quantitative comparison of entire ligandome profiles for diabetic versus control retina to systematically identify DR-associated endothelial ligands. (D) Enrichment of DR-high Scg3 and DR-low HRP-3. VEGF and GFP are internal positive and negative controls, respectively. ***, $P < 0.001$; diabetic versus healthy; χ^2 test. (E) Binding activity plot for diabetic versus healthy retina. DR-associated ligands with increased or decreased binding to diabetic endothelium are classified as DR high or DR low, respectively. Non–DR-associated ligands and background binding showed similar binding activities in both conditions. DR-high Scg3, DR-low HRP-3, non–DR-associated VEGF, and background GFP are indicated. Pearson correlation coefficient: $r = 0.489$. (F) Diabetic mice develop retinal vascular leakage. C57BL/6 mice were treated with STZ to induce diabetes. Hyperglycemic mice were aged for 4 mo to develop DR. Retinal vascular leakage was analyzed by EB assay. Data are normalized against healthy mice treated with mock buffer. $n = 12$ mice. Data are ±SEM. One-way ANOVA was used. The experiment was repeated three times. (G) Phage enrichment by in vivo binding selection. The selection scheme is showed in A. Total phage bound to retinal endothelium was quantified by plaque assay after each round of selection. (A–E and G) Ligandomics was performed once.

inal endothelium. However, a plot of the χ^2 value versus the binding activity ratio for diabetes/control uncovered many ligands with minimal, albeit statistically significant, changes in binding activity between the two conditions (Fig. 2 E). To improve the reliability of identifying disease-associated ligands, we further defined DR-high or DR-low ligands with the following more stringent, arbitrary criteria: $P < 0.001$, diabetes/control binding activity ratio ≥ 10 or ≤ 0.1, and copy number in DR or control ≥ 30. Using these criteria, we obtained 353 DR-high and 105 DR-low ligands (Table 1). While HRP-3 was identified as a DR-low ligand, Scg3 was uncovered as a DR-high ligand with the highest binding activity ratio (1,732-fold increase) among all identified ligands (Fig. 1, D and E; and Fig. 2 D). Scg2 and CgB (i.e., Chgb) were also discovered with increased binding to diabetic retinal vessels (Table S1) but were not qualified as DR-high

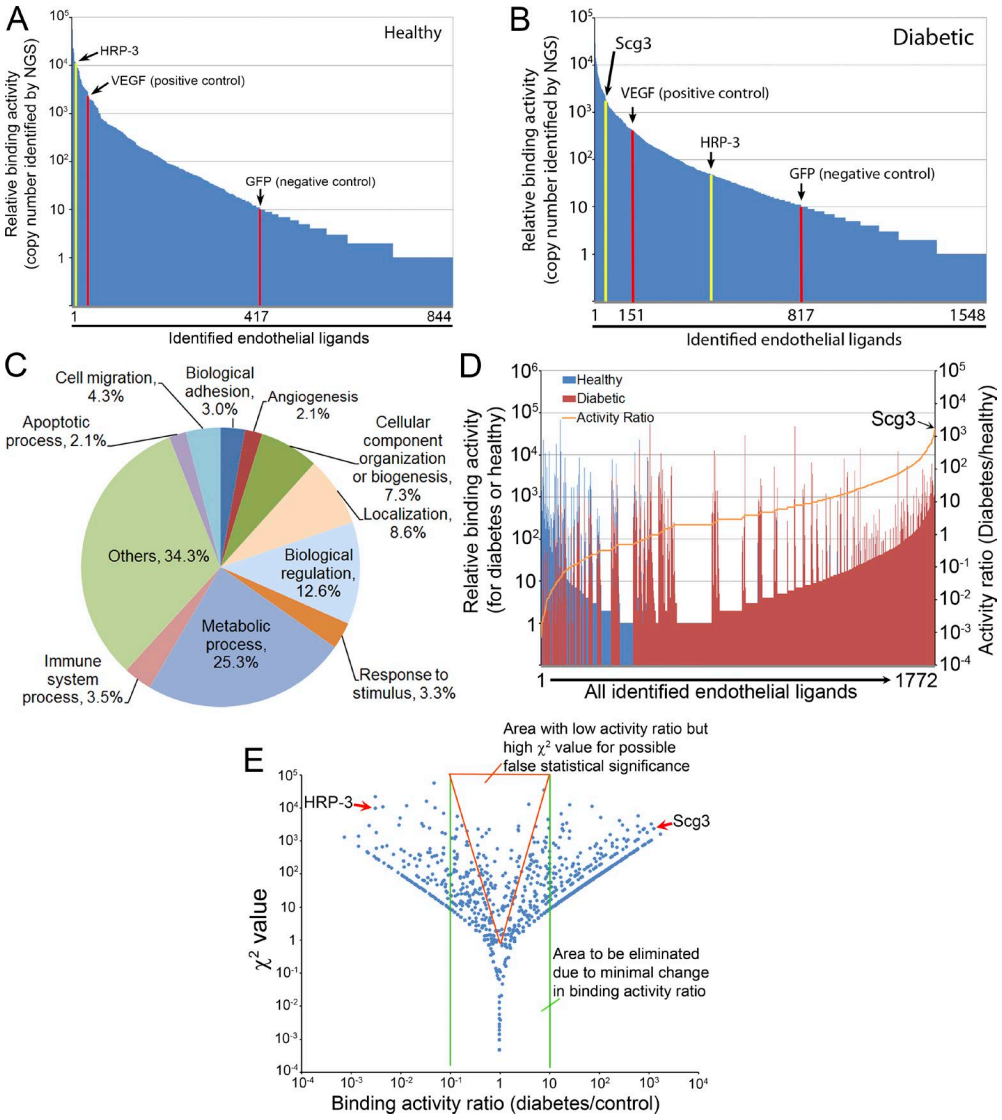

Figure 2. **Ligandomic profiling.** (A and B) Ligandome profiles. A total of 844 and 1,548 putative ligands were identified by ligandomics for control (A) and diabetic (B) retina. VEGF-Phage and GFP-Phage were internal positive and negative controls, indicated by red columns. DR-high Scg3 and DR-low HRP-3 are indicated by yellow columns. Scg3 was not detected in healthy retina. GFP is used as the baseline of nonspecific binding to distinguish 417 and 817 ligands in control and diabetic retina with binding activity higher than the background. (C) Protein classification based on their roles in biological processes. (D) Activity ratio analyses to summarize the distribution patterns of binding activity (left Y axis for vertical bars) and activity ratios (right Y axis for the orange curve) for all 1,772 nonredundant ligands identified in the two conditions. Scg3 was identified with the highest binding activity ratio. (E) χ^2 value distribution. The reliability of χ^2 test is analyzed by plotting χ^2 value against binding activity ratio. The results indicate that many ligands within the red triangle area have minimal binding activity changes but high χ^2 values, suggesting that χ^2 test alone may result in a large number of false positives. Based on this analysis, stringent criteria described in Results were used to identify 353 DR-high ligands and 105 DR-low ligands.

ligands with these criteria. We analyzed the changes in global binding activity patterns using an activity plot for all identified ligands (Fig. 1 E). The results indicated that endothelial binding activities of the entire ligandome were markedly altered in diabetic mice (Pearson correlation coefficient r = 0.498 for all 1,772 ligands).

The validity of comparative ligandomics is supported by the identification of several known and putative diabetes-associated endothelial ligands (Table 1). Amyloid β derived from amyloid precursor protein (App) is a known endothelial ligand and binds to RAGE (receptor for advanced glycation end products), which is up-regulated on diabetic endothelium (Manigrasso et al., 2014). C1qb is the β subunit of C1q complement factor that interacts with at least two endothelial receptors, cC1qR and gC1qR/p33, to produce proinflammatory cytokines (Kishore and Reid, 2000). C1q is present in significant quantities at the site of atherosclerotic lesions

(Peerschke et al., 2004), which are one of the most common diabetic vascular complications (Rask-Madsen and King, 2013). HDGF is a known mitogenic endothelial ligand (Oliver and Al-Awqati, 1998). HRP-3, in the same protein family as HDGF (Izumoto et al., 1997), was independently verified as a DR-low angiogenic factor in this study, implicating that HDGF may be a DR-low ligand as well (Table 1). Finally, receptor up-regulation on diabetic retinal endothelium for adhesion molecules, such as fibronectin 1 (Fn1), collagen type IVα3 (Col4a3), and cadherin 1 (Cdh1; Table 1), may contribute to leukocyte adhesion in DR (Rask-Madsen and King, 2013).

Independent verification of Scg3 as a novel vascular permeability and angiogenic factor

We independently verified the distinct disease association patterns of DR-high Scg3 and DR-low HRP-3. These two orphan ligands were selected because of their high-fold changes in binding activity to diabetic retinal endothelium (Fig. 1, D and E). Additionally, we recently identified HRP-3 as an angiogenic factor in healthy retina by ligandomics (LeBlanc et al., 2015).

Owing to the fact that the mouse model of STZ-induced DR developed only retinal vascular leakage but not neovascularization, we characterized Scg3 as a novel vascular permeability factor. An in vitro permeability assay showed that Scg3 significantly induced endothelial permeability from either apical or basal surfaces (Fig. 3, A–C). Similarly, VEGFRs are expressed on both the luminal and abluminal surface of ECs (Stefanini et al., 2009).

Because of the activity of Scg2-derived secretoneurin and CgA to regulate angiogenesis, we speculated that Scg3 may also be a novel angiogenic factor. This prediction was reinforced by the fact that VEGF was identified not only as an angiogenic mitogen, but also as a vascular permeability factor (Keck et al., 1989; Leung et al., 1989). We performed several functional analyses in vitro to evaluate the angiogenic activity of Scg3. The results showed that Scg3 significantly promoted the proliferation of HUVECs and human retinal microvascular ECs (HRMVECs; Fig. 3, D–F; and Fig. 7 A). Additional analyses showed that Scg3 stimulated the tube formation of ECs (Fig. 3 G). The quantification of the tube length, number of branching points, and number of the tubes confirmed that Scg3 markedly induced the tube formation (Fig. 3, H–J). Furthermore, our results revealed that Scg3 significantly promoted spheroid sprouting of HRMVECs (Fig. 7 B). A wound-healing assay indicated that Scg3 facilitated the migration of HRMVECs (Fig. 3, K and L). In all these assays, VEGF served as a positive control and significantly stimulated endothelial permeability, proliferation, tube formation, spheroid sprouting, and migration.

We characterized Scg3 expression in the retina and vitreous fluid of diabetic and control mice. Immunohistochemistry revealed that Scg3 is expressed in the retinal ganglion cells, inner and outer plexiform layers, photoreceptor inner segments, and retinal pigment epithelial cells (Fig. 4 A). Few Scg3 signals were detected in the inner and outer nuclear layers and photoreceptor outer segments. This expression pattern is consistent with its role in secretory granules to regulate neurotransmitter storage and transport (Li et al., 2012). Our results further revealed that Scg3 is expressed at a similar level in the homogenates of diabetic and control retina (Fig. 4, B and C). Scg3 secretion was verified by its presence in the vitreous fluid by Western blotting (Fig. 4 D). Interestingly, Scg3 was significantly up-regulated in the vitreous humor of 4-mo-old diabetic mice (Fig. 4, D and E), implicating that Scg3 secretion may be a regulated process, similar to the regulated secretion of CTLA-4 (Valk et al., 2008).

Table 1. **DR-associated endothelial ligands identified by comparative ligandomics**

CCDS ID	Protein	Binding activity		Activity Ratio
		DR	Control	
DR-high ligands with increased binding to diabetic ECs				
CCDS23347.1	Scg3[a]	1,731	0	1,732
CCDS18810	C1qb[a]	837	0	838
CCDS15031	Fn1[a]	419	0	420
CCDS35631	Col4a3[a]	409	2	137
CCDS28285	APP[a]	206	1	104
CCDS22638	Cdh1[a]	132	0	133
DR-low ligands with decreased binding to diabetic ECs				
CCDS40011	HRP-3[a]	48	11,140	0.0044
CCDS17457	HDGF[a]	0	83	0.0119
Internal positive and negative controls				
VEGF-Phage		408	2,420	0.1689
GFP-Phage		10	10	1
Total identified sequences		489,126	473,965	
Total identified ligands		1,548	844	
Diabetes-related ligands[a]		353↑	105↓	

[a]$P < 0.001$; DR versus control; χ^2 test. Activity ratio = (DR + 1)/(Control + 1).

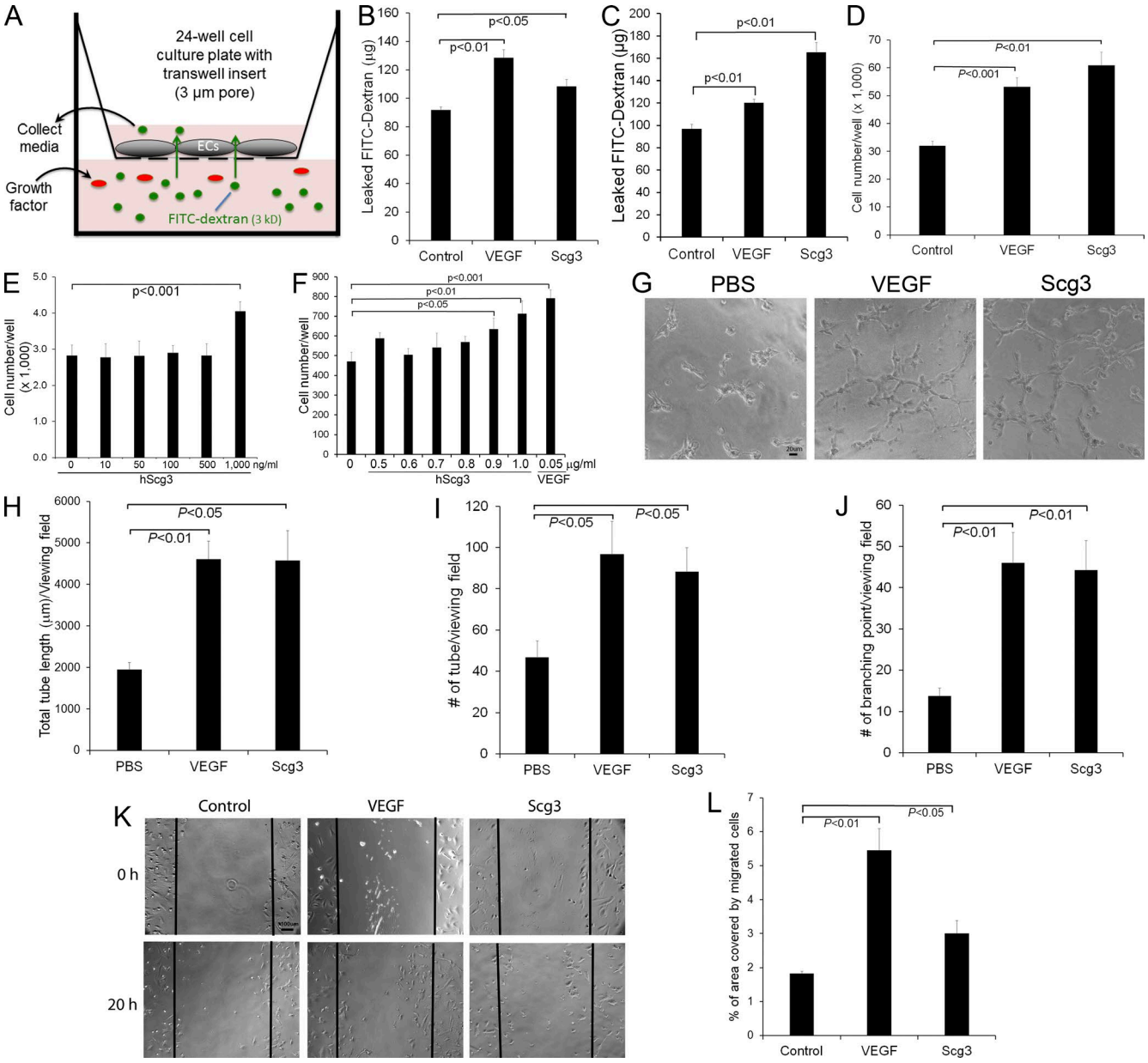

Figure 3. **In vitro characterizations of Scg3 as a novel vascular permeability and angiogenic factor.** (A–C) Scg3 promotes endothelial permeability. Permeability assay with Transwell inserts is illustrated in A. 1 µg/ml Scg3, 100 ng/ml VEGF, or PBS was added to the bottom (B) or upper (C) chamber. After 24 h, media were collected from the top chamber and quantified for leaked FITC-dextran. $n = 3$ wells. (D) Endothelial proliferation assay with HUVECs in 48-well plates. Cell number in each well was quantified at 48 h. Scg3, 1 µg/ml; VEGF, 50 ng/ml. $n = 4$ wells. (E and F) Scg3 induces endothelial proliferation only at a high concentration. HUVECs ($n = 4$ wells; E) or HRMVECs ($n = 6$; F) were incubated with increasing concentrations of Scg3 in 96-well plates for 48 h. Cells in each well were quantified. (G–J) Tube formation assay with HUVECs. (G) Representative images of the tube formation. Scg3, 300 ng/ml; VEGF, 50 ng/ml. Bar, 20 µm. (H) Total tube length per viewing field. (I) Number of tubes per viewing field. (J) Number of branching points per viewing field. $n = 4$ fields. (K and L) Scg3 stimulates the migration of HRMVECs. (K) Representative images of cell migration. Bar, 100 µm. (L) The percentage of the denuded area covered by migrated cells within the original scratch was quantified. $n = 3$. Experiments were independently repeated three times. One representative experiment is presented. Data are ±SEM. One-way ANOVA was used.

Validation of disease-high and disease-low angiogenic factors

To verify DR-high Scg3 and DR-low HRP-3 as disease-related angiogenic factors, we performed a corneal pocket assay in diabetic and control mice. We found that Scg3 preferentially induced angiogenesis in diabetic mice relative to healthy mice (Fig. 5). In contrast, HRP-3 selectively stimulated angiogenesis in healthy but not diabetic mice. As expected, a control

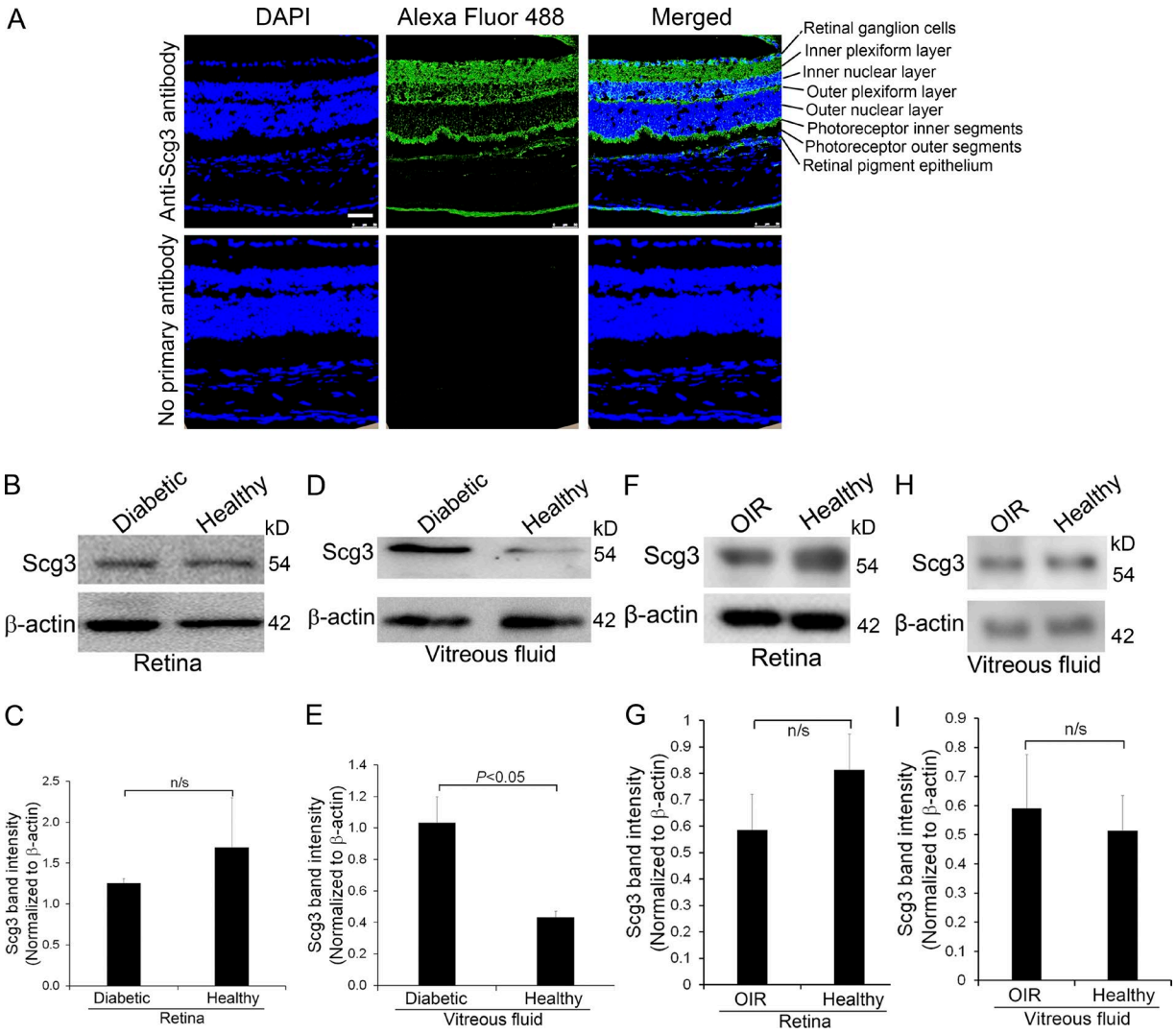

Figure 4. **Scg3 expression in the retina.** (A) Scg3 is expressed in the retinal ganglion cell layer, inner and outer plexiform layer, photoreceptor inner segments, and retinal pigment epithelial cells. Few Scg3 signals were detected in the inner and outer nuclear layer and photoreceptor outer segments. Bar, 50 µm. (B) Western blotting to detect Scg3 expression in the retina of diabetic and healthy mice. (C) Quantification of Scg3 signal in B. $n = 3$ mice. (D) Scg3 expression in the vitreous fluid of diabetic and healthy mice. (E) Quantification of Scg3 signal in D. $n = 4$ mice. (F) Scg3 expression in the retina of OIR and healthy mice at P17. (G) Quantification of Scg3 signal in F. (H) Scg3 expression in the vitreous fluid of OIR and healthy mice at P17. (I) Quantification of Scg3 signal in H. $n = 6$ mice. Experiments were repeated three times with similar results. Data are ±SEM. n/s, not significant. One-way ANOVA was used.

assay with VEGF promoted angiogenesis in both healthy and diabetic mice. These findings were not only observed by slit-lamp examination, but also verified by the staining of corneal vessels with lipophilic fluorescent DiI dye (Fig. 5, A and B). The quantification of corneal vessel number, branching points, and a comprehensive score corroborated the opposite angiogenic patterns of Scg3 and HRP-3 (Fig. 5, C–E). The quantifications also verified VEGF with similar activity in both healthy and diabetic mice (Fig. 5, C and D), except that the comprehensive score indicated more angiogenic activity for VEGF in diabetic mice than in control mice (Fig. 5 E). To our knowledge, such distinct diabetes-associated angiogenic activity patterns have not been reported previously. These data strongly suggest that Scg3 and HRP-3 are bona fide diabetes-high and diabetes-low angiogenic factors, respectively.

Different receptor signaling pathways of Scg3 and VEGF

The distinct patterns of corneal angiogenic activity in diabetic and control mice suggest that Scg3 and VEGF may have different receptors and signaling pathways. Indeed, Scg3 failed to interact with aflibercept (Fig. 6, A and B), an engineered chimeric receptor consisting of the second binding domain of VEGFR1 and the third domain of VEGFR2 fused to human IgG Fc (Holash et al., 2002). This finding was independently verified by protein pulldown and ELISA assays using VEGFR1-Fc and VEGFR2-Fc (Fig. 6, C–F). Furthermore, Scg3

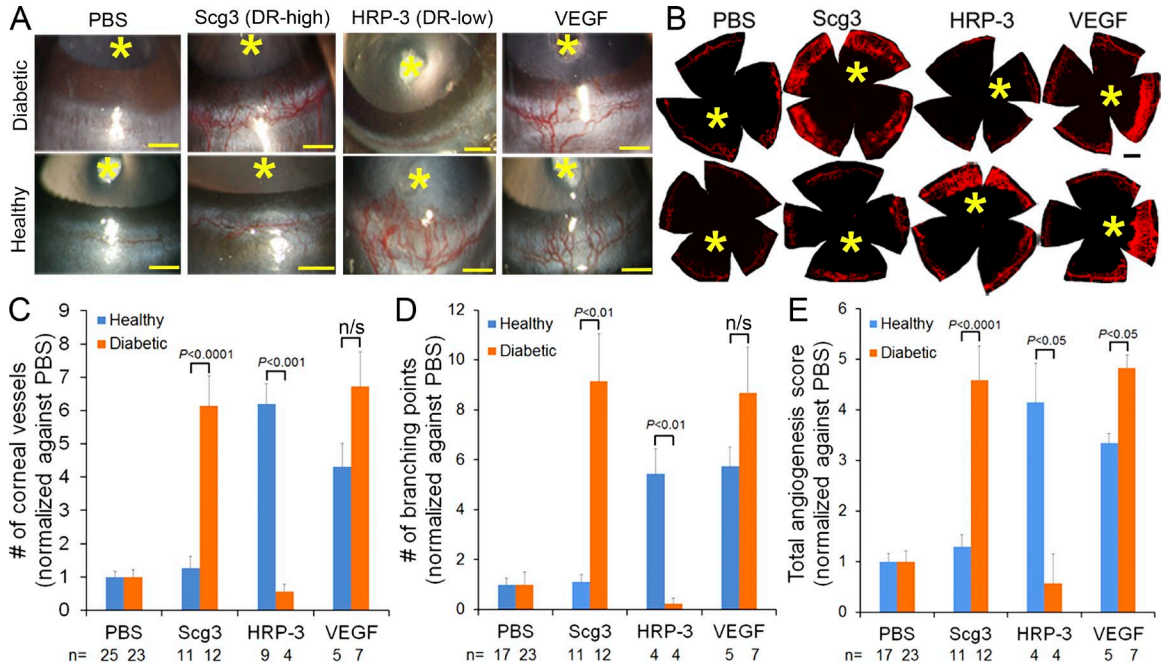

Figure 5. **Scg3 is a DR-high angiogenic factor.** (A–E) DR-high Scg3 selectively stimulated corneal angiogenesis in diabetic but not control mice. In contrast, DR-low HRP-3 induced angiogenesis in healthy but not diabetic mice. VEGF promoted angiogenesis in both healthy and diabetic mice. (A) Representative photographic images of corneal angiogenesis in diabetic and healthy mice. (B) DiI staining of corneal blood vessels. (A and B) Asterisks indicate the position of corneal implant. Bars, 500 µm. (C–E) Quantification of corneal angiogenesis in a blinded manner. (C) Total number of corneal vessels. (D) Number of branching points. (E) Total angiogenesis score. Sample sizes (number of cornea) are indicated at the bottom of the graphs. Data from different mice within the same groups are pooled and analyzed using one-way ANOVA. Data are ±SEM.

failed to activate VEGFR2 (Fig. 6 G), which is the predominant receptor for angiogenic signaling (Neufeld et al., 1999). Scg3 and VEGF activated Src (Fig. 6 H), which may induce vascular leakage through focal adhesion kinase/vascular endothelial cadherin (Cerani et al., 2013). Although both Scg3 and VEGF activated mitogen-activated protein kinase (MEK) and downstream extracellular signal–regulated kinases 1/2 (ERK1/2; Fig. 6, I and J), only VEGF, and not Scg3, stimulated the phosphorylation of Akt and Stat3 pathways (Fig. 6, K and L). These data suggest that Scg3 and VEGF with distinct receptors may partially converge their intracellular signaling to differentially regulate angiogenesis and vascular leakage.

Anti-Scg3 therapy alleviates diabetic retinal vascular leakage

Given the pathogenic role of angiogenic factors in DR (Rask-Madsen and King, 2013; Wells et al., 2015), we predicted that DR-high Scg3 may be a promising target for antiangiogenesis therapy to alleviate diabetic retinal vascular leakage. We verified that affinity-purified anti-Scg3 polyclonal antibody (pAb) is capable of blocking Scg3-induced proliferation of HRMVECs (Fig. 7 A). Anti-Scg3 pAb alone had no effect on endothelial proliferation. The neutralizing activity of the pAb was independently confirmed by spheroid sprouting assay (Fig. 7 B). Importantly, intravitreal injection of Scg3-neutralizing pAb significantly reduced DR leakage in STZ-induced diabetic mice with a similar therapeutic efficacy as aflibercept (70 and 73% reduction for anti-Scg3 and aflibercept; Fig. 7 F). As a control, mock affinity-purified pAb against an irrelevant antigen had no inhibition on DR leakage. These findings uncovered Scg3 as a promising target for antiangiogenesis therapy of DME.

Anti-Scg3 therapy of retinal angiogenesis

In contrast to diabetic patients who may develop PDR 10–20 yr after the disease onset (Yau et al., 2012), diabetic rodents do not progress toward PDR, probably because of their relatively short lifespan. Oxygen-induced retinopathy (OIR) is an animal model of ROP and has been widely used as a surrogate model of proliferative retinopathy with angiogenesis (Stahl et al., 2010; Kim et al., 2016). We investigated whether anti-Scg3 therapy may prevent retinal neovascularization induced by OIR. Intravitreal injection of Scg3-neutralizing pAb prevented OIR-induced pathological neovascularization characterized by neovascular tufts and tortuous blood vessels (Fig. 8 A). The quantification of vessel density, neovascular tufts, and vessel branching points indicated that anti-Scg3 significantly inhibited OIR-induced neovascularization (Fig. 8, B–D). Similar therapeutic effects were also observed for aflibercept. These data implicate the therapeutic potential of anti-Scg3 for ROP and PDR patients.

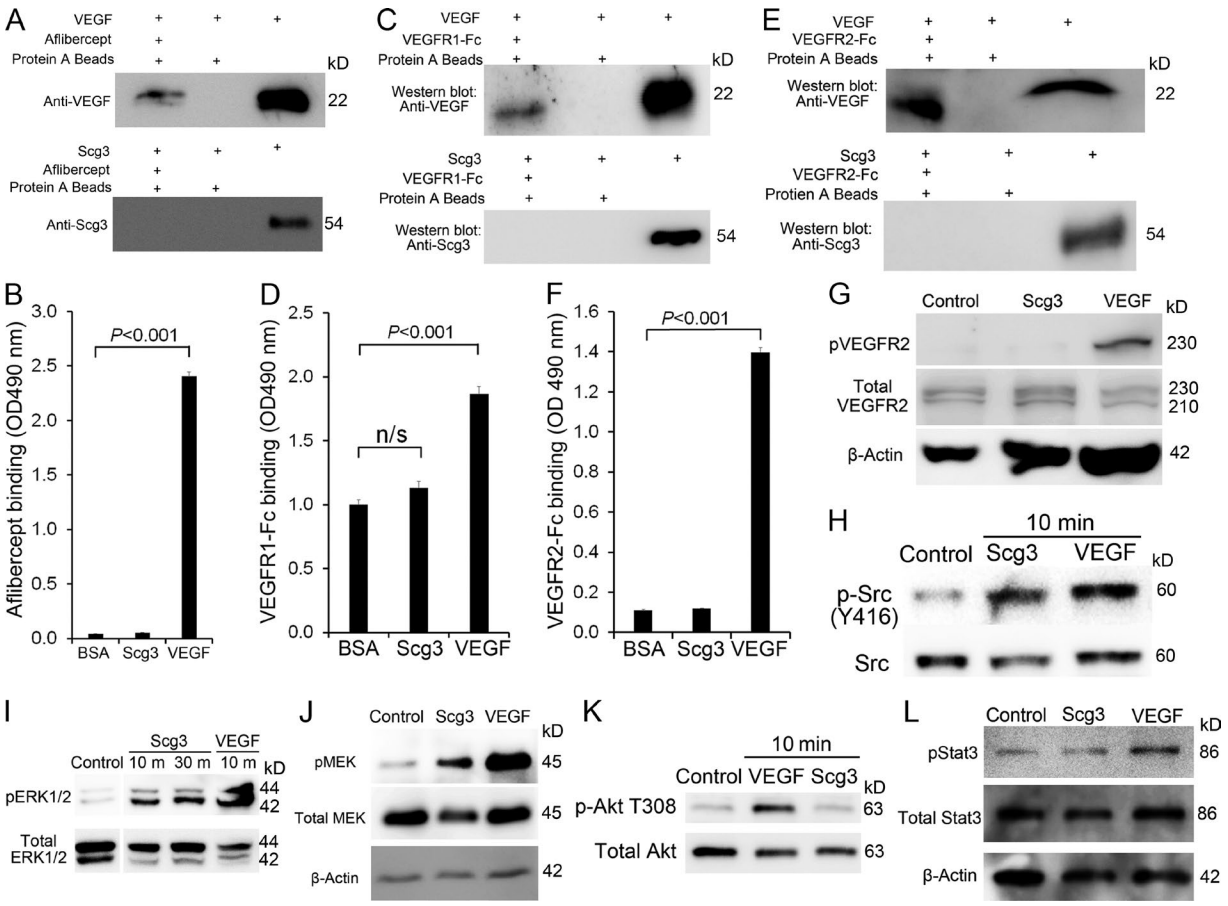

Figure 6. **Scg3 and VEGF have distinct receptor signaling pathways.** (A–F) Scg3 does not bind to VEGFR1 or VEGFR2. Protein pulldown (A, C, and E) and ELISA (B, D, and F) assays failed to detect Scg3 interaction with aflibercept (A and B), VEGFR1-Fc (C and D), or VEGFR2-Fc (E and F). $n = 3$ wells. Data are ±SEM. One-way ANOVA was used. (G) Scg3 does not activate VEGFR2 in HRMVECs. (H–J) Scg3 and VEGF activate Src (H), ERK1/2 (I), and MEK (J) in HUVECs. (K and L) VEGF, but not Scg3, induces the phosphorylation of Akt and Stat3. Experiments were independently repeated three times.

Independent validation of anti-Scg3 therapy

However, despite affinity purification and various controls, pAb may nonspecifically recognize other proteins with off-target effects. Unlike pAb, mAbs minimally cross react with other proteins and are well recognized as selective reagents for target validation as well as therapy. We developed an anti-Scg3 mAb (clone ML49.3) and characterized its capacity to neutralize Scg3-induced proliferation of HRMVECs (Fig. 7 C). Anti-Scg3 mAb cannot inhibit VEGF-induced proliferation of HRMVECs (Fig. 7 D). Furthermore, ML49.3 mAb recognized both human and mouse Scg3 (Fig. 7 E), which share 88.3% identity in amino acid sequence. Intravitreal injection of Scg3-neutralizing mAb alleviated retinal vascular leakage in STZ-induced diabetic mice (Fig. 7 F), suggesting that Scg3 is a bona fide target for antiangiogenic therapy of DR.

$Ins2^{Akita}$ mice with a missense mutation in the insulin 2 gene spontaneously develop type 1 diabetes (Wang et al., 1999) and were used to independently verify the therapeutic efficacy of anti-Scg3 mAb. The mice develop retinal vascular leakage at 6 mo of age (Han et al., 2013). Intravitreal injection of anti-Scg3 mAb significantly inhibited retinal leakage in $Ins2^{Akita}$ mice with a similar efficacy to aflibercept (Fig. 7 G), corroborating Scg3 as a target for DR therapy.

In addition, intravitreal injection of anti-Scg3 mAb prevented pathological retinal neovascularization in OIR mice with high efficacy (Fig. 8), suggesting that Scg3 is a potential target for antiangiogenic therapy of PDR and ROP.

DISCUSSION

Comparative ligandomics to identify disease-associated ligands

Cellular ligands extrinsically regulate a broad spectrum of physiological and pathological functions, such as proliferation, apoptosis, differentiation, adhesion, migration, secretion, phagocytosis, and immune response. Several ligands with protective or detrimental roles have been overexpressed or blocked to successfully treat different diseases (Pardoll, 2012; Weissmiller and Wu, 2012; Vasudev and Reynolds, 2014). It is estimated that between one third and one half of all marketed drugs act by binding to cellular ligands or receptors,

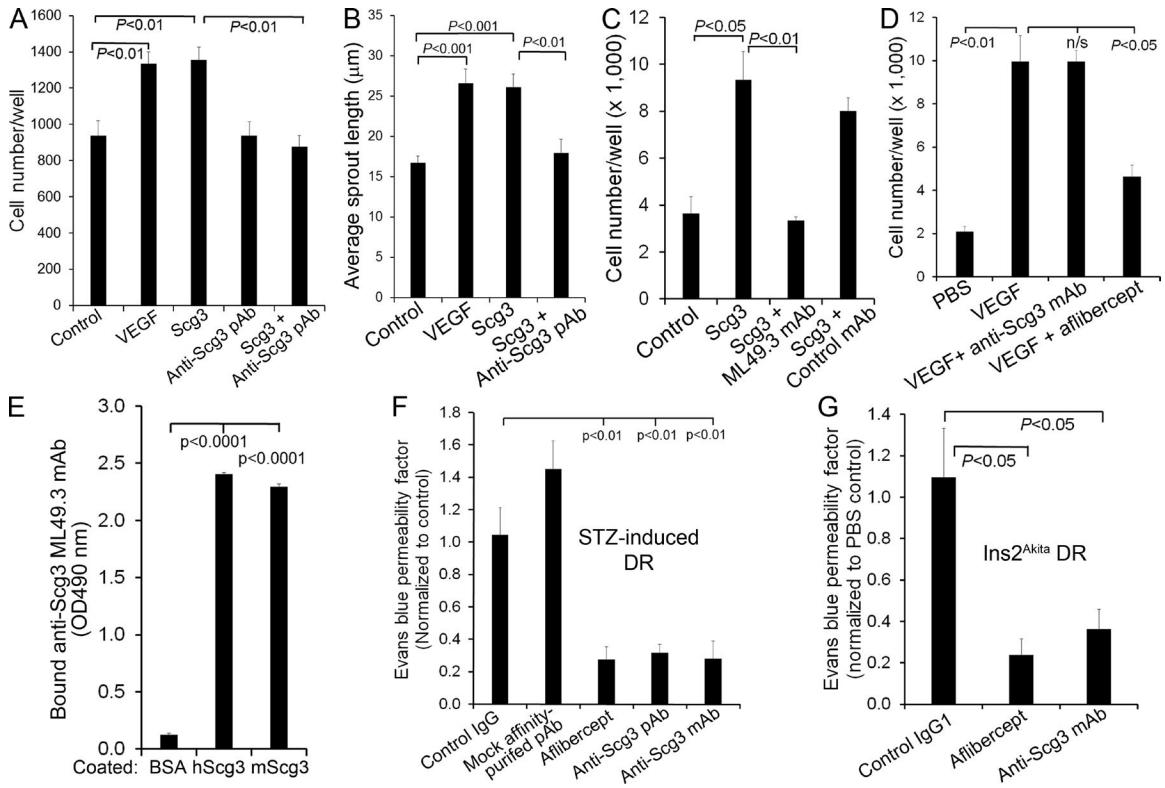

Figure 7. **Anti-Scg3 therapy of DR.** (A) Affinity-purified anti-Scg3 pAb blocks Scg3-induced proliferation of HRMVECs. VEGF, 100 ng/ml; Scg3, 1 µg/ml; anti-Scg3 pAb, 2 µg/ml. *n* = 8 wells. (B) Anti-Scg3 pAb inhibits Scg3-induced spheroid sprouting of HRMVECs. VEGF, 2.5 ng/ml; Scg3, 15 ng/ml; anti-Scg3 pAb, 30 ng/ml. *n* = 8 spheroids. (C) Anti-Scg3 ML49.3 mAb inhibits Scg3-induced HRMVEC proliferation. Concentrations are as in A. *n* = 3 wells. (D) Anti-Scg3 mAb cannot neutralize VEGF-induced proliferation of HRMVECs. *n* = 3 wells. (E) ML49.3 mAb binds to both human Scg3 (hScg3) and mouse Scg3 (mScg3) as detected by ELISA assay. *n* = 3 wells. (F) Anti-Scg3 therapy of DR in STZ-induced diabetic mice. Anti-Scg3 pAb, mock affinity-purified pAb against an irrelevant antigen, control rabbit IgG, ML49.3 mAb (0.36 µg/1 µl/eye), aflibercept (2 µg/1 µl/eye), or PBS was intravitreally injected. Retinal vascular leakage was quantified by EB assay. Data are normalized to PBS. *n* = 5 mice (except *n* = 3 for mock pAb). (G) Anti-Scg3 therapy of DR in $Ins2^{Akita}$ diabetic mice. Doses are as in F. *n* = 3 mice (4 for anti-Scg3). Experiments were independently repeated three times (A–E) or were repeated twice in a blinded manner (F and G). One representative experiment is shown. Data are ±SEM. One-way ANOVA was used.

such as G protein–coupled receptors (Sodhi et al., 2004). The bottleneck of developing novel ligand-based therapies is how to efficiently identify ligands with pathogenic roles and therapeutic potential.

We have recently reported the first paradigm of ligandomics, which was initially designed to globally identify only cell-wide ligands (Ding et al., 2015; Guo et al., 2015; LeBlanc et al., 2015). To map pathogenic or therapeutic ligands, this study established the reliability for ligandomics to globally quantify ligand-binding activity. We further applied this approach to systematically delineate disease-associated ligands with altered binding in the disease state. The opposite angiogenic activity patterns of DR-high Scg3 and DR-low HRP-3 in Fig. 5 support the validity of comparative ligandomics. The successful demonstration of anti-Scg3 therapy for DR corroborates the utility of this new approach. Collectively, these findings support the concept that global profiling of the binding activity of the entire ligandome is a useful approach to systematically identify disease-associated ligands (Fig. 9 A). This approach can be extended to define the pathogenic contributions and therapeutic potential of disease-associated ligands, which may accelerate or delay disease pathogenesis depending on the context.

The major advantage of comparative ligandomics is demonstrated by DR-high Scg3. Disease-high ligands with relatively low binding activities to healthy cells are likely to be overlooked by conventional ligand-screening approaches. As a result, Scg3 has never been reported as an angiogenic factor. This analysis can efficiently screen for disease-high ligands, followed by additional functional analyses in healthy and diseased cells or conditions.

Scg3 was identified as a DR-high ligand by ligandomics with 1,731 and 0 copies in diabetic and healthy retina, respectively (Fig. 1, D and E; and Table 1). These numbers will increase or decrease in parallel based on the total number of sequences analyzed by NGS. Therefore, undetected Scg3 binding to healthy retinal endothelium likely does not indicate the absolute absence of Scg3 receptors but, rather, suggests their

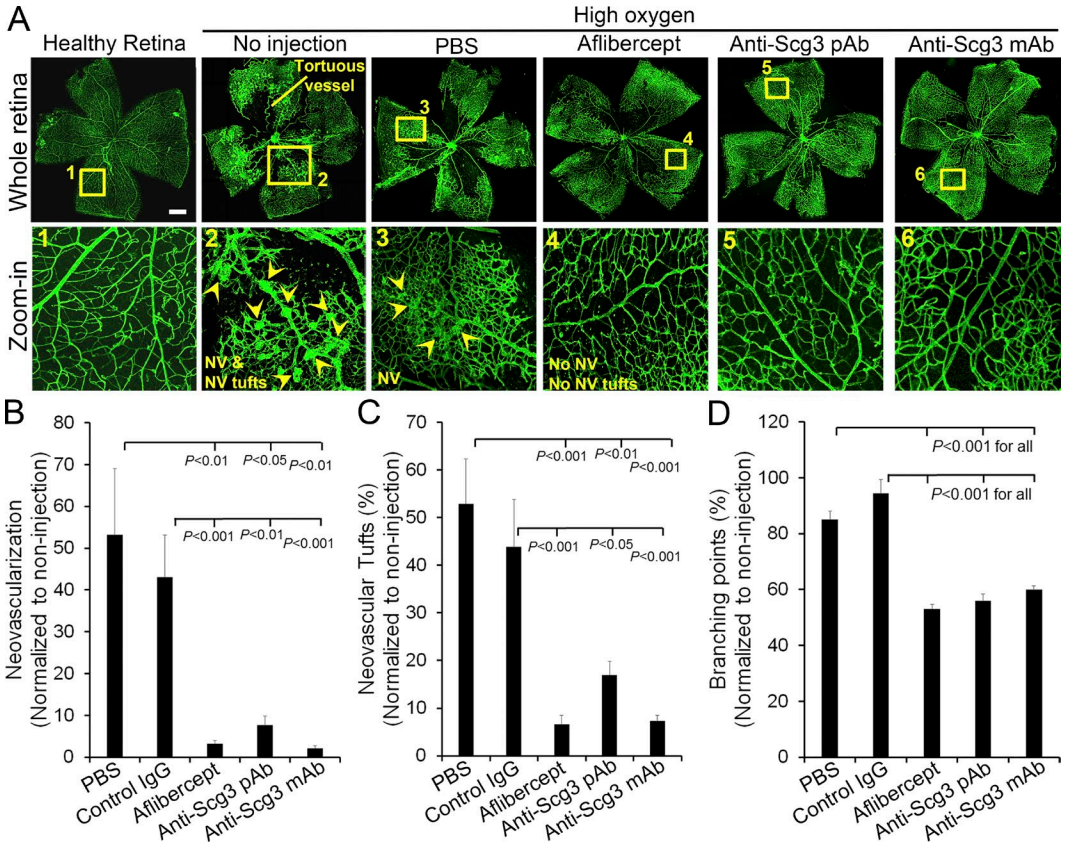

Figure 8. **Anti-Scg3 therapy of OIR.** (A) Representative images of OIR. Arrowheads indicate neovascularization (NV) and neovascularization tufts. Doses are as in Fig. 7 F. Bar, 500 µm. (B) Quantification of neovascularization. (C) Quantification of neovascularization tuft number. (D) Quantification of branching points. n = 13 (PBS), 11 (control IgG), 12 (aflibercept), 11 (anti-Scg3 pAb), and 13 (anti-Scg3 mAb) eyes. This experiment was repeated twice in a blinded manner. Data are ±SEM. One-way ANOVA was used.

relatively low expression. Indeed, weak Scg3 angiogenic activity, albeit not statistically significant, was detected by in vivo angiogenesis assay in healthy cornea (Scg3 vs. PBS; Fig. 5, C and E). Furthermore, Scg3 is capable of stimulating HUVECs and HRMVECs at a relatively high dose (Fig. 3, E and F), consistent with Scg3 regulation of nondiabetic ECs by other functional assays (Fig. 3, and Fig. 7, A–C).

Although the up-regulation of pathogenic ligands, such as VEGF, may trigger disease (Aiello et al., 1994), altered receptor expression can also contribute to disease pathogenesis with therapeutic opportunity. One of the well-known examples is the down-regulation of insulin receptor in type 2 diabetes despite the elevated level of insulin. This study focused on systematic profiling of ligands with increased or decreased binding to diseased vasculature, rather than with altered expression. Scg3 was discovered with at least a 1,731-fold increase in binding to diabetic retinal endothelium (1,731:0 for diabetes/control; Fig. 1 D). In contrast, Scg3 expression was moderately up-regulated by only 1.38-fold (Fig. 4 E), suggesting that increased binding of Scg3 is mainly responsible for its pathogenic role in DR. Although Scg3 expression was not up-regulated in OIR (Fig. 4, F–I), anti-Scg3 mAb was capable of preventing OIR with high efficacy (Fig. 8), implicating possible increase in Scg3 binding to OIR vasculature. Once the Scg3 receptor is identified, increased binding of Scg3, rather than its expression, in DR or OIR should be independently verified before clinical trials of anti-Scg3 therapy.

A major limitation of OPD-based ligandomics is that mammalian ligands expressed in bacteria may not always have proper protein folding or glycosylation. Ligandomics is developed to systematically delineate the majority of disease-related ligands but not to exhaustively identify every possible ligand. The critical issue is whether this technical problem will limit the applicability of ligandomics only to a small percentage of cellular ligands. We randomly surveyed hundreds of functionally active extracellular soluble ligands, such as growth factors (e.g., VEGF, epidermal growth factor, and fibroblast growth factor), cytokines, and chemotactic proteins, commercially available from Thermo Fisher Scientific and Abcam. About 80–88% of ligands can be expressed in bacteria and purified as active ligands without problems in protein folding or posttranslational modifications. Glycosylation is important to VEGF secretion but not its functional activity (Buchholz et al., 2008). Even Scg3 with putative glycosylation (Holthuis

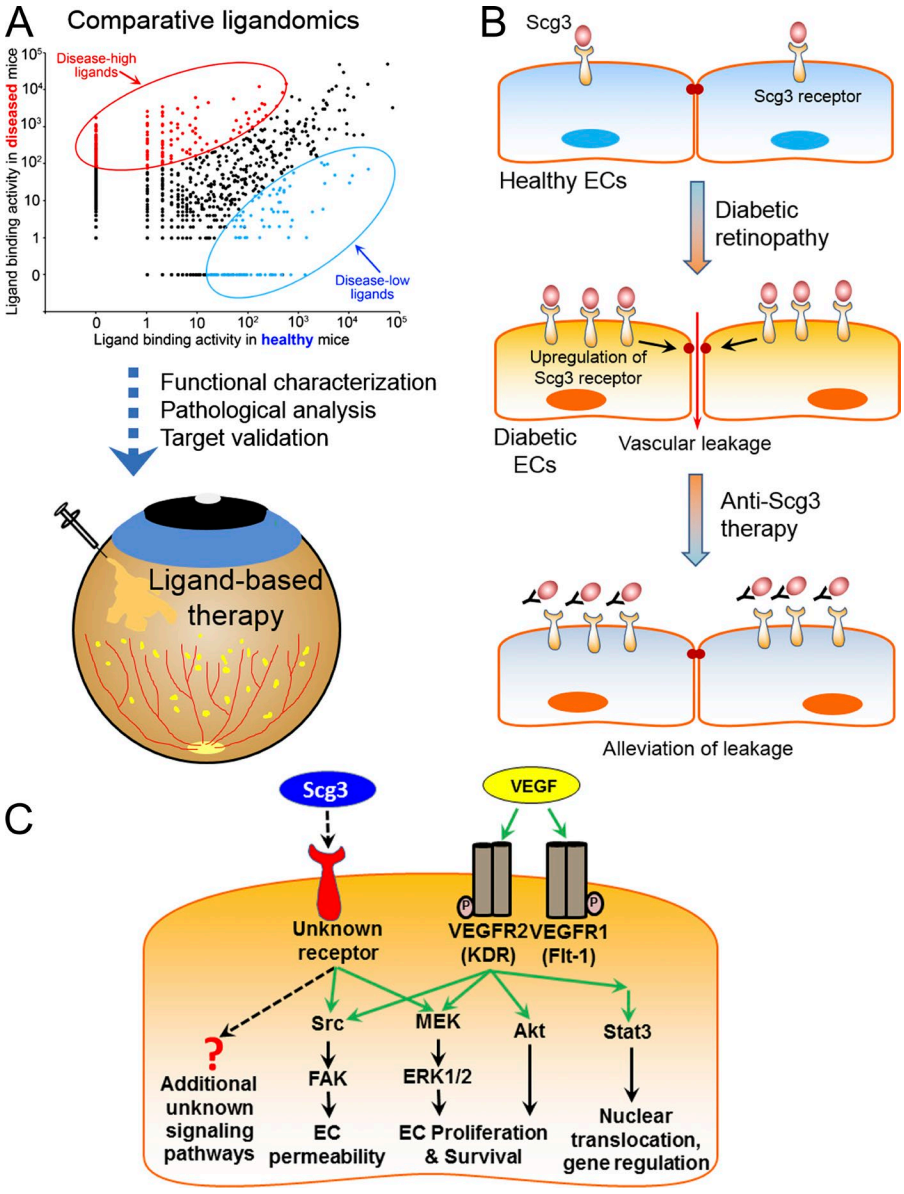

Figure 9. **Schematic models of comparative ligandomics, anti-Scg3 therapy, and Scg3 molecular mechanisms.** (A) From comparative ligandomics to ligand-based therapy. This study encompasses the initial ligand screening, functional characterization, pathogenic analysis, target validation, and ligand-based therapy to demonstrate the validity and utility of comparative ligandomics. (B) Anti-Scg3 therapy. Scg3 is a unique angiogenic factor that minimally regulates normal ECs. The marked up-regulation of its receptors on diabetic ECs coupled with moderate Scg3 up-regulation in diabetic vitreous exacerbates retinal vascular leakage in DR. Scg3-neutralizing antibody alleviates the leakage by blocking Scg3 binding to its receptor. (C) Scg3 molecular mechanisms. Scg3 activates ERK and Src pathways, but not Akt and Stat3, through unknown receptors. ERK activated by Scg3 and VEGF may regulate different metabolic events (see the Scg3 as a disease-associated angiogenic ligand section of Discussion). FAK, focal adhesion kinase.

et al., 1996; Rong et al., 2002), probably in the nonreceptor-binding domain, can be identified by ligandomics in this study. Therefore, despite possibly missing a small percentage of ligands, ligandomics should be applicable to delineate many physiologically relevant cellular ligands.

An intriguing question is whether DR leakage may nonspecifically affect in vivo binding selection. Increased vascular permeability may allow the leakage of proteins up to 2,000 kD (Egawa et al., 2013). T7 phage is a bacterial virus consisting of a few hundred copies of different proteins and a 37-kb genome. Its size of ~55 nm in diameter is equivalent to a protein with ~90,000 kD. Thus, phages were not expected to leak within 20-min in vivo selection. Furthermore, nonreceptor-mediated events should have similar effects on all phage clones and could not preferentially enrich any specific ones. The differential enrichment of hVEGF-Phage versus GFP-Phage in diabetic mice supports the feasibility and reliability of receptor-mediated in vivo binding selection (Fig. 1 D).

Of note, ligandomics is broadly applicable to any type of cell or disease in in vitro or in vivo settings through different ligand enrichment strategies, including binding and functional selections (Ding et al., 2015; Guo et al., 2015; LeBlanc et al., 2015). Disease-associated cellular ligands identified by this approach will facilitate the development of novel ligand-based therapies, as illustrated in this study.

Scg3 as a disease-associated angiogenic ligand

Scg3 was initially identified as a product of the mouse 1B1075 gene, which is predominantly expressed in the brain (Ottiger et al., 1990). Scg3 is now considered a member of the granin

family because of its hydrophilic acidic amino acid composition and characteristic localization to the secretory granules in endocrine cells. Scg3 is largely characterized as a regulator for the biogenesis of secretory granules and the secretion of hormone peptides in endocrine and neuroendocrine cells (Hosaka and Watanabe, 2010). Scg3 binds to the CgA, cholesterol-rich membrane domain of the trans-Golgi network and membrane-associated carboxypeptidase E (Hosaka et al., 2002, 2005). The binding stoichiometric ratio of Scg3 to CgA is 1:11 (Han et al., 2008). It is proposed that Scg3 functions as a linker molecule by tethering microaggregates of prohormones and CgA to a cholesterol-rich domain of the trans-Golgi network (Hosaka and Watanabe, 2010). In parallel, Scg3 recruits processing enzymes, such as carboxypeptidase E, to strengthen this assembly of the membrane-associated complex. However, Scg3 is not essential for the secretion of hormones and neurotransmitters because $Scg3^{-/-}$ mice have a normal phenotype (Kingsley et al., 1990).

Scg3 is up-regulated in several tumors, including neuroendocrine tumors, small-cell lung cancer, prostate cancer, and hepatocellular carcinoma (Jongsma et al., 2002; Moss et al., 2009; Portela-Gomes et al., 2010; Wang et al., 2014). However, the functional role of Scg3 in tumorigenesis has never been characterized. Scg3 with a classical signal peptide can be secreted into conditioned medium from dysfunctional β cells and, therefore, may be up-regulated in type 1 diabetes (Dowling et al., 2008), consistent with our finding (Fig. 4 E). However, secreted Scg3 has never been described as an extrinsic regulator for any cell.

This study discovered Scg3 as a disease-associated angiogenic factor. Anti-Scg3 therapy of diabetic retinal leakage suggests that Scg3 is a pathogenic ligand in DR. These data implicate that Scg3 has minimal binding and angiogenic activity in normal vessels but markedly increases its binding and angiogenic activity in DR.

Given that ranibizumab and aflibercept have been approved for DR therapy, why do we need to develop another antiangiogenic therapy against Scg3? Anti-VEGF therapies have moderate therapeutic efficacy (Nguyen et al., 2012). Owing to limited therapeutic options, DME patients with a poor response to one anti-VEGF drug are often switched to another VEGF inhibitor (Hanhart and Chowers, 2015), despite their similar mechanisms of action. Antiangiogenic therapies targeting different signaling pathways could facilitate alternative or combination therapy of anti-VEGF–resistant DR. Additionally, there is no approved drug therapy for PDR. Anti-Scg3 therapy can address these unmet clinical needs (Fig. 9 B).

VEGF is crucial to vascular and retinal development at embryonic and neonatal stages. Mice with a homozygous deletion of either VEGFR1 or 2 die in the uterus (Fong et al., 1995; Shalaby et al., 1995). Similarly, mice with the deletion of a single *VEGF* allele are embryonically lethal (Ferrara et al., 1996). In all VEGF or VEGFR knockout mice, premature death was attributed to severe defect in vasculogenesis, which could in turn affect embryogenesis. Anti-VEGF therapy of ROP in preterm infants was associated with adverse side effects (Lepore et al., 2014; Beharry et al., 2016). Because of the uncertainty in efficacy and safety, VEGF inhibitors were not approved for ROP therapy. Our results showed that anti-Scg3 therapy had high efficacy for OIR. The high disease selectivity of Scg3 implicates that anti-Scg3 therapy may have minimal side effects on normal vessels. This notion is supported by the reported normal phenotype of mice with homozygous deletion of the *Scg3* gene (i.e., equivalent to 100% Scg3 blockade; Kingsley et al., 1990), suggesting minimal adverse effects on vasculogenesis and embryogenesis. However, anti-Scg3 antibody should be thoroughly characterized for any adverse effects on the developing vasculature and retina before clinical translation. Scg3 binding to OIR versus normal neonatal vessels should be quantified and compared using ligandomics as in this study.

A previous study reported that aflibercept increased the avascular area in OIR mice (Tokunaga et al., 2014). However, our results indicated that both anti-Scg3 mAb and aflibercept did not enlarge the avascular region (unpublished data). This may be attributed to differences in the OIR timeline and doses of aflibercept between the experiments.

We addressed the enigma of Scg3 molecular mechanisms in Fig. 6. Scg3 activated ERK and Src pathways, but not Akt and Stat3, to regulate angiogenesis and vascular leakage (Fig. 9 C). The mechanistic studies in Fig. 6 serve two important purposes: (1) to verify Scg3 as a bona fide endothelial ligand capable of activating intracellular signaling cascades and (2) to determine whether Scg3 and VEGF have different receptor pathways. ERK and Src can be activated by different receptors, including receptor tyrosine kinases (e.g., VEGFRs), G protein–coupled receptors, or integrins (Ramos, 2008; Huveneers and Danen, 2009; Koch et al., 2011; Lappano and Maggiolini, 2011). Thus, we speculate that Scg3 may activate a non-VEGFR receptor. The subcellular location of activated ERK determines the downstream signaling cascade and cellular response (Eishingdrelo and Kongsamut, 2013). Perhaps this may explain why either anti-Scg3 or anti-VEGF alone substantially inhibited DR leakage (Fig. 7, F and G) and OIR neovascularization (Fig. 8).

Of particular interest is the identification of Scg3 receptors, which will facilitate not only the verification of its up-regulation in DR, but also development of an aflibercept-like decoy receptor for alternative anti-Scg3 therapy. The Scg3-neutralizing mAb characterized in this study could be a valuable tool for the receptor identification. However, the challenge to identify the receptor is complicated by its minimal expression on normal ECs. Nonetheless, based on the distinct angiogenic activity patterns, we demonstrated that Scg3 and VEGF have different receptor signaling pathways. VEGF has three receptors, VEGFR1, 2, and 3. The first two receptors play a key role in angiogenesis (Robinson and Stringer, 2001), whereas VEGFR3 involves in lymphangiogenesis (Neufeld et al., 1999). We independently verified that Scg3 does not bind

to VEGFR1 and 2 by protein pulldown and ELISA (Fig. 6, A–F). Moreover, Scg3 cannot activate VEGFR2 (Fig. 6 G), the predominant receptor for angiogenic signaling (Neufeld et al., 1999). These data suggest that Scg3 and VEGF have different spectra of angiogenic activity, supporting alternative or combination therapy for DR with their inhibitors.

The observed 1,731-fold increase in Scg3 binding to diabetic retinal endothelium provides an important disease correlation for anti-Scg3 therapy. Similar to VEGF up-regulation in PDR patients (Aiello et al., 1994), our results revealed a moderate increase in vitreous Scg3 of diabetic mice (Fig. 4 E). This finding should be verified for disease correlation in PDR patients. These results suggest that both marked increase in Scg3 endothelial binding and moderate up-regulation of vitreous Scg3 may contribute to DR pathogenesis.

In summary, we performed high-throughput screening by comparative ligandomics, systematically identified disease-associated ligands, independently verified their distinct mechanisms and activity patterns, and demonstrated a novel ligand-based therapy (Fig. 9). Scg3 was characterized as a novel disease-associated angiogenic factor and a promising target for the therapy of DME, PDR, and ROP. Humanized Scg3 mAb for bench-to-bedside translation may offer the advantages of disease selectivity, high efficacy, minimal side effects, and a distinct signaling pathway. These advantages are yet to be fully investigated in animal models and clinical trials.

MATERIALS AND METHODS

Materials

Human VEGF165 (no. 293-VE-010/CF), VEGFR1-Fc (no. 321-FL-050/FC), and VEGFR2-Fc (no. 357-KD-050/FC) were from R&D Systems. Amicon centrifugal filter units (no. UFC501008) were from EMD Millipore. Affinity-purified anti-Scg3 pAb (no. 10954-1-AP), anti-Plekha1 pAb (no. 10238-1-AP), and anti-VEGFR2 (no. 26415-1-AP) were from Proteintech. Anti-ERK1/2 (no. 9102), anti-pERK1/2 (no. 4377), anti-Akt (no. 4691), anti-pAkt T308 (no. 13038), anti-pMEK (no. 23385), anti-MEK (no. 9126), anti-pStat3 (no. 9145), anti-Stat3 (no. 12640), anti-Src (no. 2110), anti-pSrc (no. 2101), anti-pVEGFR2 (Y1175; no. 2478s), and anti–β-actin (no. 4967) were from Cell Signaling Technology. Alexa Fluor 488–conjugated isolectin B4 (no. I21411) was from Thermo Fisher Scientific. Whatman filter paper (grade 3; no. 1003-090) was from GE Healthcare. Evans blue (EB; no. 2129), DiI (no. 42364), STZ (no. S0130), FITC-dextran (no. FD4), and protein G beads (no. P7700) were from Sigma-Aldrich. High concentration growth factor reduced Matrigel (no. 354263) was from Corning. Recombinant HRP-3 was prepared as previously described (LeBlanc et al., 2015). Anti-Scg3 mAb (clone ML49.3; mouse IgG1) was raised against the full-length human Scg3 (Sino Biological) by Creative Biolabs through a subcontract service and purified from serum-free hybridoma-conditioned medium using protein G columns (Kim et al., 2011). Mouse IgG1 was purified from the conditioned medium of 9E10 hybridoma (Developmental Studies Hybridoma Bank). Control rabbit IgG was purified from rabbit serum (Sigma-Aldrich).

Diabetic mice

C57BL/6 mice (6 wk old, male; The Jackson Laboratory) were induced for type 1 diabetes with STZ or mock citrate buffer, as previously described (Zhong et al., 2012). Male mice tend to be more susceptible to STZ-induced diabetes (Deeds et al., 2011). In brief, mice were starved for 4 h and then received STZ (40 µg/g body weight) or sodium citrate buffer (137 mM, pH 4.5) via intraperitoneal injection for five consecutive days. STZ was dissolved in the citrate buffer (7.5 mg/ml) immediately before the injection. Mice were monitored for blood glucose biweekly and considered diabetic when blood glucose was ≥350 mg/dl, usually starting at 2 wk after STZ treatment. Hyperglycemic mice were aged for 4 mo to develop DR. To avoid human bias, therapeutic agents for all in vivo studies were coded in a blinded manner, as indicated in the figure legends. All animal procedures were approved by the Institutional Animal Care and Use Committee at the University of Miami.

Heterozygous male $Ins2^{Akita}$ (C57BL/6-$Ins2^{Akita}$) mice (no. 003548; The Jackson Laboratory) were bred with wild-type C57BL/6 female mice. Heterozygous $Ins2^{Akita}$ males, which developed hyperglycemia by 4–6 wk of age, were monitored for blood glucose. The diabetic phenotype and associated complications were more severe and progressive in the males than in females. $Ins2^{Akita}$ males developed retinal vascular leakage at 6 mo of age and therefore were chosen for this study.

OIR mice

OIR was induced as previously described (Connor et al., 2009; LeBlanc et al., 2016). In brief, mice (C57BL/6; male and female) at postnatal day 7 (P7) were exposed to 75% oxygen in a regulated chamber. At P12, anti-Scg3 pAb, control IgG, anti-Scg3 mAb, aflibercept, or PBS was intravitreally injected into anesthetized mice, which were returned to room air after the injection. At P17, mice were euthanized by CO_2 inhalation. Isolated retinas were stained with Alexa Fluor 488–isolectin B4, flat-mounted, and analyzed by confocal microscopy. Neovascularization and related tufts were quantified as previously described (Connor et al., 2009). Additionally, the number of branching points within a defined area was quantified in the same region of each retina. All data were normalized against noninjection OIR eyes.

Cell culture

HUVECs, HRMVECs, and their culture conditions were previously described (LeBlanc et al., 2015, 2016).

Clonal phages

Clonal phages were constructed as previously described (Caberoy et al., 2009b). In brief, the coding sequences of GFP was amplified by PCR, digested, and cloned into a T7Bio3C

phage vector (Caberoy et al., 2010) at NotI and XhoI sites to generate GFP-Phage. The coding sequence for wild-type $hVEGF_{1–110}$ with artificial codons was designed as in Fig. S1, commercially synthesized (GenScript), and cloned into T7Bio3C at NotI and XhoI sites to generate hVEGF-Phage. Both clonal phages were verified by sequencing.

In vivo binding selection

OPD libraries derived from mouse adult eyes and E18 embryos were described previously (Caberoy et al., 2009a, 2010). NGS analysis of unselected libraries indicated that the combined libraries consist of at least 9,500 different proteins. The OPD libraries and control clonal phages were amplified and purified (LeBlanc et al., 2015). hVEGF-Phage and GFP-Phage in equal titers were diluted into the pooled libraries at a 1:1,000 ratio. The mixed libraries were intravenously injected into STZ-induced diabetic mice (three mice/group/round; 10^{12} PFU/mouse) and circulated for 20 min (LeBlanc et al., 2015). Unbound phages were removed by intracardial perfusion with PBS. Retinas were isolated and homogenized in PBS containing 1% Triton X-100 to release endothelium-bound phages. Aliquots of the lysates were used to quantify phage titer by plaque assay (Caberoy et al., 2009b). The remaining phages in the lysates were amplified, repurified, and used as the input for the next round of in vivo selection. After three rounds of selection, the cDNA inserts of enriched phage clones were amplified by PCR, purified from agarose gel (400–1,500 bp), and identified by NGS (LeBlanc et al., 2015).

Comparative ligandomic data analysis

NGS data were aligned against the NCBI CCDS database to identify enriched ligands. The copy numbers of cDNA inserts identified by NGS represent the relative binding activities of their cognate ligands to retinal endothelium and were quantitatively compared by χ^2 test to identify DR-associated ligands as follows.

All identified ligands and their copy numbers (i.e., counts) for diabetic and control retina were compiled into a single Excel spreadsheet. Each identified ligand has two copy numbers, one for diabetic retina (diabetic_count) and the other for control retina (control_count). The statistical analysis for individual ligands was calculated with the following formula in Excel: $Chi = ($a × $d − $b × $c) × ($a × $d − $b × $c) × ($a + $b + $c + $d)/[($a + $b) × ($b + $d) × ($a + $c) × ($d + $c)], where $a = $diabetic_count; $b = $control_count; $c = $total_diabetic_count − $a; $d = $total_control_count − $b; and $total_diabetic_count and $total_control_count are total copy numbers of NGS reads matched for diabetic and control retina. In this study, $total_diabetic_count is 489,126, and $total_control_count is 473,965. Thus, $c = 489,126 − $a and $d = 473,965 − $b.

The p-value was calculated from χ^2 value ($Chi) with the following formula in Excel: p-value = CHIDIST($Chi, 1).

To calculate the binding activity ratios, the copy numbers of individual ligands were normalized against total valid reads identified by NGS. Normalized read of an individual ligand in control retina = $b × $total_diabetic_count/$total_control_count. With the above total counts for diabetic and control retinas in this study, the formula was simplified as: normalized read of individual ligand in control retina = 1.03 × $b. The adjustment is negligible. After data normalization, the activity ratio = (DR + 1)/(Control + 1), as described in Table 1.

CCDS ID of NGS data were batch-converted to UniProt accession nos. and analyzed by the PANTHER Classification System and DAVID database. Identified ligands were categorized based on the gene ontology terms Cellular Component and Biological Process.

Endothelial permeability assay

The assay was performed in vitro as previously described (Martins-Green et al., 2008). In brief, HUVECs were plated in Transwell inserts in 24-well plates and cultured to confluence. 1 mg/ml FITC-dextran (3–5 kD) was added to the bottom chamber along with Scg3, VEGF, or PBS. After 24 h, FITC concentration in the upper chamber was quantified and calculated against a standard curve.

Cell proliferation assay

HRMVECs or HUVECs at four to eight passages were cultured with Scg3, VEGF165, or PBS in 96- or 48-well plates as previously described (LeBlanc et al., 2015). When needed, anti-Scg3 pAb or mAb was washed three times with PBS in Amicon centrifugal filter units (10 kD cutoff), concentrated, and added to cells. Fresh medium, growth factors, and antibody were added every 24 h. Cells in each well were collected by trypsin digestion at 48 h, resuspended in PBS with 1 mM trypan blue, and quantified.

Tube formation assay

The assay was described previously (LeBlanc et al., 2015). In brief, HUVECs were starved in serum-free EBM-2 medium (Lonza) overnight, harvested, and plated on Matrigel-coated 96-well plates at 15,000 cells/well. Cells were incubated with Scg3, VEGF, or PBS in EBM-2 medium at 37°C for 4 h. Bright field images were taken. Total tube length, number of tubes, and number of branching points per viewing field were quantified using ImageJ software (National Institutes of Health).

Wound-healing assay

Cell migration was analyzed by in vitro wound-healing assay as previously described (LeBlanc et al., 2015). In brief, HRMVECs were cultured in 12-well plates to near confluence and starved in EBM-2 medium with 0.2% FBS for 3 h. A scratch was created in each well with a 200-µl tip. After rinsing, cells were cultured with Scg3 or VEGF. Cell migration into the scratched area was monitored at 0 and 20 h by phase-contrast microscopy. The percentage of the denuded area covered by migrated cells within the original scratch was quantified using ImageJ.

Spheroid sprouting

The assay was performed with HRMVECs as previously described (LeBlanc et al., 2015). In brief, HRMVECs were cultured in nonadhesive 96-well round-bottom plates with 20% Methocel solution and 10% FBS for 24 h to form spheroids. Spheroids were harvested, embedded in the fibrin gel, and incubated with Scg3, VEGF, or PBS with or without anti-Scg3 mAb in EBM-2 medium for 48 h. Photographs were taken using a phase-contrast microscope, and mean sprout lengths were quantified using ImageJ.

Protein pulldown

5 µg/ml Scg3 or VEGF was incubated with 5 µg/ml aflibercept, VEGFR1-Fc, or VEGFR2-Fc in PBS solution containing 0.5% Triton X-100 and 1 mg/ml BSA for 1 h at 4°C. 20 µl of protein G beads was added and incubated at 4°C for 30 min with end-over-end rotation. Beads were washed three times with PBS by centrifugation, eluted with low-pH buffer (100 mM glycine, pH 2.7), and analyzed by Western blotting using anti-Scg3 pAb or anti-VEGF antibody.

Cell signaling

The phosphorylation of Src, MEK, ERK1/2, Akt, and Stat3 was detected as previously described (LeBlanc et al., 2015). HUVECs were preincubated in serum-free EBM-2 medium for 15 min three times at 37°C to reduce the effect of other growth factors. Cells were incubated with 1 µg/ml Scg3 and 100 ng/ml VEGF or PBS in EBM-2 medium for 10 or 30 min at 37°C, lysed, and analyzed by Western blotting using antibody against phosphorylated proteins, specific proteins, or β-actin.

VEGFR2 activation

VEGFR2 activation was detected as previously described (Jin et al., 2003). HRMVECs were incubated with 100 ng/ml VEGF, 1 µg/ml Scg3, or PBS for 24 h. After washing, cells were collected, lysed, and analyzed by Western blotting using antibody against phosphorylated VEGFR2, total VEGFR2, or β-actin.

Immunohistochemistry

Immunohistochemical analysis of mouse retina was performed using affinity-purified anti-Scg3 pAb as previously described (Guo et al., 2015). In brief, frozen retinal sections in 7-µm thickness were incubated with anti-Scg3 pAb, followed by Alexa Fluor 488–labeled goat anti–rabbit IgG antibody. The nuclei were visualized with DAPI. Signals were analyzed by confocal microscopy.

Scg3 expression in the retina and vitreous fluid

The vitreous fluid in equal volume (1.5 µl/eye) was collected from 4-mo-old diabetic and age-matched control mice and subjected to Western blot assay. Their retinas were isolated and homogenized in SDS-PAGE loading buffer. Samples were analyzed by Western blotting using anti-Scg3 pAb or anti–β-actin antibody (Angayarkanni et al., 2009; Murthy et al., 2014).

ELISA

Human and mouse Scg3 were immobilized on ELISA plates, blocked, and incubated with anti-Scg3 mAb. Bound mAbs were detected by horseradish peroxidase–conjugated secondary antibody using colorimetric assay, as previously described (Caberoy et al., 2010).

Corneal angiogenesis assay

The assay was performed as previously described (LeBlanc et al., 2015). In brief, sterilized Whatman filter paper (grade 3) was cut into pieces (0.125 mm^2/piece) and soaked in the solution of 0.25 µg/µl Scg3, 0.1 µg/µl VEGF165, and 1 µg/µl HRP-3 or PBS for 2 h at 4°C. Soaked papers were implanted into corneal pockets of anesthetized C57BL/6 mice (8 wk old; one paper/cornea; fellow eyes always for PBS). After 6 d, corneal angiogenesis was evaluated using a slit-lamp microscope and photographed. The number of new sprouting vessels into the cornea and their branching points and semiquantitative score were quantified and normalized against PBS in fellow eyes (LeBlanc et al., 2015). Then, mice were euthanized by CO_2 and immediately perfused intracardially with fluorescent DiI dye. Flat-mounted corneas were analyzed by confocal microscopy to detect DiI-labeled blood vessels.

EB assay

Retinal vascular leakage was quantified by EB assay as previously described (Scheppke et al., 2008; LeBlanc et al., 2016). In brief, antibodies were washed three times in Amicon centrifugal filter units (10 kD) with PBS and concentrated. Affinity-purified anti-Scg3 pAb, affinity-purified pAb against an irrelevant antigen (Plekha1; mock control), rabbit control IgG, anti-Scg3 mAb, mouse control IgG1, or aflibercept was intravitreally injected into one eye of diabetic mice with PBS for contralateral eyes. EB was intravenously injected, circulated for 2.5 h, and intracardially perfused. Retinas were isolated 4 h after therapy and incubated with formamide at 70°C overnight to extract EB, which was quantified at 620 and 740 nm (background) and compared with a standard curve. Blood samples were collected from EB-injected mice before intracardial perfusion, directly centrifuged at 3,550 *g* for 15 min at 25°C, diluted, and quantified at the same wavelengths. EB leakage was calculated with the following formula: (leaked EB concentration [mg/ml]/retinal weight [mg])/(blood EB concentration [mg/ml] × circulation time [h]). Data are normalized to PBS in fellow eyes and expressed as percentage of reduction in leakage.

Statistical analysis

Data are expressed as mean ± SEM. Intergroup differences were analyzed using ANOVA with a Tukey posthoc test or a two-tailed Student's *t* test. NGS datasets were compared by χ^2 test.

Online supplemental material

Table S1 shows known or putative endothelial ligands identified by comparative ligandomics. Fig. S1 shows the sequences for hVEGF-Phage with altered codons but wild-type protein sequence.

ACKNOWLEDGMENTS

We thank Keith Webster, Philip Rosenfeld, Jian-Xing Ma, Henry Flynn, and William Smiddy for scientific advice and discussion; Feng Wang for NGS data analysis; William Feuer for advice on statistical analysis; Gabriela Alvarado, Akhalesh Shakya, Chenming Zhang, Robert Liu, and Jisu Yu for technical help; Gabriel Gaidosh for confocal service; Megan Brewer for cartoon drawing; Fanglian Zhang and Ron Wen for instrument support; and Pickersgill and Andersen (Life Science Editors) and Abigail Hackam for manuscript editing.

This work was supported by the National Institutes of Health (grants. R01GM094449, R21HD075372, and R21EY027065 to W. Li and grant P30-EY014801), BrightFocus Foundation (grant M2012026 to W. Li), an institutional grant and a Special Scholar Award (W. Li) from Research to Prevent Blindness, and an American Heart Association Predoctoral Fellowship (14PRE18310014 and 16PRE27250308 to M.E. LeBlanc).

Patent applications are pending.

W. Li, H. Tian, and M.E. LeBlanc are the founders and shareholders of Everglades Biopharma. The authors declare no further competing financial interests.

Submitted: 25 October 2016

Revised: 23 December 2016

Accepted: 15 February 2017

REFERENCES

Aiello, L.P., R.L. Avery, P.G. Arrigg, B.A. Keyt, H.D. Jampel, S.T. Shah, L.R. Pasquale, H. Thieme, M.A. Iwamoto, J.E. Park, et al. 1994. Vascular endothelial growth factor in ocular fluid of patients with diabetic retinopathy and other retinal disorders. *N. Engl. J. Med.* 331:1480–1487. http://dx.doi.org/10.1056/NEJM199412013312203

Angayarkanni, N., R. Selvi, R. Pukhraj, J. Biswas, S.J. Bhavesh, and J. Tombran-Tink. 2009. Ratio of the vitreous vascular endothelial growth factor and pigment epithelial-derived factor in Eales disease. *J. Ocul. Biol. Dis. Infor.* 2:20–28. http://dx.doi.org/10.1007/s12177-009-9017-7

Beharry, K.D., G.B. Valencia, D.R. Lazzaro, and J.V. Aranda. 2016. Pharmacologic interventions for the prevention and treatment of retinopathy of prematurity. *Semin. Perinatol.* 40:189–202. http://dx.doi.org/10.1053/j.semperi.2015.12.006

Buchholz, C.J., L.J. Duerner, S. Funke, and I.C. Schneider. 2008. Retroviral display and high throughput screening. *Comb. Chem. High Throughput Screen.* 11:99–110. http://dx.doi.org/10.2174/138620708783744543

Caberoy, N.B., Y. Zhou, G. Alvarado, X. Fan, and W. Li. 2009a. Efficient identification of phosphatidylserine-binding proteins by ORF phage display. *Biochem. Biophys. Res. Commun.* 386:197–201. http://dx.doi.org/10.1016/j.bbrc.2009.06.010

Caberoy, N.B., Y. Zhou, and W. Li. 2009b. Can phage display be used as a tool to functionally identify endogenous eat-me signals in phagocytosis? *J. Biomol. Screen.* 14:653–661. http://dx.doi.org/10.1177/1087057109335679

Caberoy, N.B., Y. Zhou, X. Jiang, G. Alvarado, and W. Li. 2010. Efficient identification of tubby-binding proteins by an improved system of T7 phage display. *J. Mol. Recognit.* 23:74–83.

Cerani, A., N. Tetreault, C. Menard, E. Lapalme, C. Patel, N. Sitaras, F. Beaudoin, D. Leboeuf, V. De Guire, F. Binet, et al. 2013. Neuron-derived semaphorin 3A is an early inducer of vascular permeability in diabetic retinopathy via neuropilin-1. *Cell Metab.* 18:505–518. http://dx.doi.org/10.1016/j.cmet.2013.09.003

Connor, K.M., N.M. Krah, R.J. Dennison, C.M. Aderman, J. Chen, K.I. Guerin, P. Sapieha, A. Stahl, K.L. Willett, and L.E. Smith. 2009. Quantification of oxygen-induced retinopathy in the mouse: a model of vessel loss, vessel regrowth and pathological angiogenesis. *Nat. Protoc.* 4:1565–1573. http://dx.doi.org/10.1038/nprot.2009.187

Coppinger, J.A., G. Cagney, S. Toomey, T. Kislinger, O. Belton, J.P. McRedmond, D.J. Cahill, A. Emili, D.J. Fitzgerald, and P.B. Maguire. 2004. Characterization of the proteins released from activated platelets leads to localization of novel platelet proteins in human atherosclerotic lesions. *Blood.* 103:2096–2104. http://dx.doi.org/10.1182/blood-2003-08-2804

Deeds, M.C., J.M. Anderson, A.S. Armstrong, D.A. Gastineau, H.J. Hiddinga, A. Jahangir, N.L. Eberhardt, and Y.C. Kudva. 2011. Single dose streptozotocin-induced diabetes: considerations for study design in islet transplantation models. *Lab. Anim.* 45:131–140. http://dx.doi.org/10.1258/la.2010.010090

Ding, Y., N.B. Caberoy, F. Guo, M.E. LeBlanc, C. Zhang, W. Wang, F. Wang, R. Chen, and W. Li. 2015. Reticulocalbin-1 facilitates microglial phagocytosis. *PLoS One.* 10:e0126993. http://dx.doi.org/10.1371/journal.pone.0126993

Dowling, P., W. Shields, S. Rani, P. Meleady, M. Henry, P. Jeppesen, L. O'Driscoll, and M. Clynes. 2008. Proteomic analysis of conditioned media from glucose responsive and glucose non-responsive phenotypes reveals a panel of secreted proteins associated with beta cell dysfunction. *Electrophoresis.* 29:4141–4149. http://dx.doi.org/10.1002/elps.200800152

Egawa, G., S. Nakamizo, Y. Natsuaki, H. Doi, Y. Miyachi, and K. Kabashima. 2013. Intravital analysis of vascular permeability in mice using two-photon microscopy. *Sci. Rep.* 3:1932. http://dx.doi.org/10.1038/srep01932

Eishingdrelo, H., and S. Kongsamut. 2013. Minireview: Targeting GPCR activated ERK pathways for drug discovery. *Curr. Chem. Genomics Transl. Med.* 7:9–15. http://dx.doi.org/10.2174/2213988501307010009

Ferrara, N., K. Carver-Moore, H. Chen, M. Dowd, L. Lu, K.S. O'Shea, L. Powell-Braxton, K.J. Hillan, and M.W. Moore. 1996. Heterozygous embryonic lethality induced by targeted inactivation of the VEGF gene. *Nature.* 380:439–442. http://dx.doi.org/10.1038/380439a0

Fong, G.H., J. Rossant, M. Gertsenstein, and M.L. Breitman. 1995. Role of the Flt-1 receptor tyrosine kinase in regulating the assembly of vascular endothelium. *Nature.* 376:66–70. http://dx.doi.org/10.1038/376066a0

Guariguata, L., D.R. Whiting, I. Hambleton, J. Beagley, U. Linnenkamp, and J.E. Shaw. 2014. Global estimates of diabetes prevalence for 2013 and projections for 2035. *Diabetes Res. Clin. Pract.* 103:137–149. http://dx.doi.org/10.1016/j.diabres.2013.11.002

Guo, F., Y. Ding, N. Caberoy, G. Alvarado, F. Wang, R. Chen, and W. Li. 2015. ABCF1 extrinsically regulates retinal pigment epithelial cell phagocytosis. *Mol. Biol. Cell.* 26:2311–2320. http://dx.doi.org/10.1091/mbc.E14-09-1343

Han, L., M. Suda, K. Tsuzuki, R. Wang, Y. Ohe, H. Hirai, T. Watanabe, T. Takeuchi, and M. Hosaka. 2008. A large form of secretogranin III functions as a sorting receptor for chromogranin A aggregates in PC12 cells. *Mol. Endocrinol.* 22:1935–1949. http://dx.doi.org/10.1210/me.2008-0006

Han, Z., J. Guo, S.M. Conley, and M.I. Naash. 2013. Retinal angiogenesis in the $Ins2^{Akita}$ mouse model of diabetic retinopathy. *Invest. Ophthalmol. Vis. Sci.* 54:574–584. http://dx.doi.org/10.1167/iovs.12-10959

Hanhart, J., and I. Chowers. 2015. Evaluation of the response to ranibizumab therapy following bevacizumab treatment failure in eyes with diabetic macular edema. *Case Rep. Ophthalmol.* 6:44–50. http://dx.doi.org/10.1159/000375230

Helle, K.B., and A. Corti. 2015. Chromogranin A: a paradoxical player in angiogenesis and vascular biology. *Cell. Mol. Life Sci.* 72:339–348. http://dx.doi.org/10.1007/s00018-014-1750-9

Holash, J., S. Davis, N. Papadopoulos, S.D. Croll, L. Ho, M. Russell, P. Boland, R. Leidich, D. Hylton, E. Burova, et al. 2002. VEGF-Trap: a VEGF blocker with potent antitumor effects. *Proc. Natl. Acad. Sci. USA.* 99:11393–11398. http://dx.doi.org/10.1073/pnas.172398299

Holthuis, J.C., E.J. Jansen, and G.J. Martens. 1996. Secretogranin III is a sulfated protein undergoing proteolytic processing in the regulated secretory pathway. *J. Biol. Chem.* 271:17755–17760. http://dx.doi.org/10.1074/jbc.271.30.17755

Hosaka, M., and T. Watanabe. 2010. Secretogranin III: a bridge between core hormone aggregates and the secretory granule membrane. *Endocr. J.* 57:275–286. http://dx.doi.org/10.1507/endocrj.K10E-038

Hosaka, M., T. Watanabe, Y. Sakai, Y. Uchiyama, and T. Takeuchi. 2002. Identification of a chromogranin A domain that mediates binding to secretogranin III and targeting to secretory granules in pituitary cells and pancreatic β-cells. *Mol. Biol. Cell.* 13:3388–3399. http://dx.doi.org/10.1091/mbc.02-03-0040

Hosaka, M., T. Watanabe, Y. Sakai, T. Kato, and T. Takeuchi. 2005. Interaction between secretogranin III and carboxypeptidase E facilitates prohormone sorting within secretory granules. *J. Cell Sci.* 118:4785–4795. http://dx.doi.org/10.1242/jcs.02608

Huveneers, S., and E.H. Danen. 2009. Adhesion signaling - crosstalk between integrins, Src and Rho. *J. Cell Sci.* 122:1059–1069. http://dx.doi.org/10.1242/jcs.039446

Izumoto, Y., T. Kuroda, H. Harada, T. Kishimoto, and H. Nakamura. 1997. Hepatoma-derived growth factor belongs to a gene family in mice showing significant homology in the amino terminus. *Biochem. Biophys. Res. Commun.* 238:26–32. http://dx.doi.org/10.1006/bbrc.1997.7233

Jin, Z.G., H. Ueba, T. Tanimoto, A.O. Lungu, M.D. Frame, and B.C. Berk. 2003. Ligand-independent activation of vascular endothelial growth factor receptor 2 by fluid shear stress regulates activation of endothelial nitric oxide synthase. *Circ. Res.* 93:354–363. http://dx.doi.org/10.1161/01.RES.0000089257.94002.96

Jongsma, J., M.H. Oomen, M.A. Noordzij, W.M. Van Weerden, G.J. Martens, T.H. van der Kwast, F.H. Schröder, and G.J. van Steenbrugge. 2002. Different profiles of neuroendocrine cell differentiation evolve in the PC-310 human prostate cancer model during long-term androgen deprivation. *Prostate.* 50:203–215. http://dx.doi.org/10.1002/pros.10049

Keck, P.J., S.D. Hauser, G. Krivi, K. Sanzo, T. Warren, J. Feder, and D.T. Connolly. 1989. Vascular permeability factor, an endothelial cell mitogen related to PDGF. *Science.* 246:1309–1312. http://dx.doi.org/10.1126/science.2479987

Kim, C.B., P.A. D'Amore, and K.M. Connor. 2016. Revisiting the mouse model of oxygen-induced retinopathy. *Eye Brain.* 8:67–79. http://dx.doi.org/10.2147/EB.S94447

Kim, Y., N.B. Caberoy, G. Alvarado, J.L. Davis, W.J. Feuer, and W. Li. 2011. Identification of Hnrph3 as an autoantigen for acute anterior uveitis. *Clin. Immunol.* 138:60–66. http://dx.doi.org/10.1016/j.clim.2010.09.008

Kingsley, D.M., E.M. Rinchik, L.B. Russell, H.P. Ottiger, J.G. Sutcliffe, N.G. Copeland, and N.A. Jenkins. 1990. Genetic ablation of a mouse gene expressed specifically in brain. *EMBO J.* 9:395–399.

Kirchmair, R., M. Egger, D.H. Walter, W. Eisterer, A. Niederwanger, E. Woell, M. Nagl, M. Pedrini, T. Murayama, S. Frauscher, et al. 2004. Secretoneurin, an angiogenic neuropeptide, induces postnatal vasculogenesis. *Circulation.* 110:1121–1127. http://dx.doi.org/10.1161/01.CIR.0000139884.81390.56

Kishore, U., and K.B. Reid. 2000. C1q: structure, function, and receptors. *Immunopharmacology.* 49:159–170. http://dx.doi.org/10.1016/S0162-3109(00)80301-X

Koch, S., S. Tugues, X. Li, L. Gualandi, and L. Claesson-Welsh. 2011. Signal transduction by vascular endothelial growth factor receptors. *Biochem. J.* 437:169–183. http://dx.doi.org/10.1042/BJ20110301

Lappano, R., and M. Maggiolini. 2011. G protein-coupled receptors: novel targets for drug discovery in cancer. *Nat. Rev. Drug Discov.* 10:47–60. http://dx.doi.org/10.1038/nrd3320

LeBlanc, M.E., W. Wang, N.B. Caberoy, X. Chen, F. Guo, G. Alvarado, C. Shen, F. Wang, H. Wang, R. Chen, et al. 2015. Hepatoma-derived growth factor-related protein-3 is a novel angiogenic factor. *PLoS One.* 10:e0127904. http://dx.doi.org/10.1371/journal.pone.0127904

LeBlanc, M.E., W. Wang, X. Chen, Y. Ji, A. Shakya, C. Shen, C. Zhang, V. Gonzalez, M. Brewer, J.X. Ma, et al. 2016. The regulatory role of hepatoma-derived growth factor as an angiogenic factor in the eye. *Mol. Vis.* 22:374–386.

Lepore, D., G.E. Quinn, F. Molle, A. Baldascino, L. Orazi, M. Sammartino, V. Purcaro, C. Giannantonio, P. Papacci, and C. Romagnoli. 2014. Intravitreal bevacizumab versus laser treatment in type 1 retinopathy of prematurity: report on fluorescein angiographic findings. *Ophthalmology.* 121:2212–2219. http://dx.doi.org/10.1016/j.ophtha.2014.05.015

Leung, D.W., G. Cachianes, W.J. Kuang, D.V. Goeddel, and N. Ferrara. 1989. Vascular endothelial growth factor is a secreted angiogenic mitogen. *Science.* 246:1306–1309. http://dx.doi.org/10.1126/science.2479986

Li, W. 2012. ORF phage display to identify cellular proteins with different functions. *Methods.* 58:2–9. http://dx.doi.org/10.1016/j.ymeth.2012.07.013

Li, F., X. Tian, Y. Zhou, L. Zhu, B. Wang, M. Ding, and H. Pang. 2012. Dysregulated expression of secretogranin III is involved in neurotoxin-induced dopaminergic neuron apoptosis. *J. Neurosci. Res.* 90:2237–2246. http://dx.doi.org/10.1002/jnr.23121

Manigrasso, M.B., J. Juranek, R. Ramasamy, and A.M. Schmidt. 2014. Unlocking the biology of RAGE in diabetic microvascular complications. *Trends Endocrinol. Metab.* 25:15–22. http://dx.doi.org/10.1016/j.tem.2013.08.002

Martins-Green, M., M. Petreaca, and M. Yao. 2008. An assay system for in vitro detection of permeability in human "endothelium". *Methods Enzymol.* 443:137–153. http://dx.doi.org/10.1016/S0076-6879(08)02008-9

Mintz-Hittner, H.A., K.A. Kennedy, and A.Z. Chuang. BEAT-ROP Cooperative Group. 2011. Efficacy of intravitreal bevacizumab for stage 3+ retinopathy of prematurity. *N. Engl. J. Med.* 364:603–615. http://dx.doi.org/10.1056/NEJMoa1007374

Moss, A.C., G.M. Jacobson, L.E. Walker, N.W. Blake, E. Marshall, and J.M. Coulson. 2009. SCG3 transcript in peripheral blood is a prognostic biomarker for REST-deficient small cell lung cancer. *Clin. Cancer Res.* 15:274–283. http://dx.doi.org/10.1158/1078-0432.CCR-08-1163

Murthy, K.R., R. Goel, Y. Subbannayya, H.K. Jacob, P.R. Murthy, S.S. Manda, A.H. Patil, R. Sharma, N.A. Sahasrabuddhe, A. Parashar, et al. 2014. Proteomic analysis of human vitreous humor. *Clin. Proteomics.* 11:29. http://dx.doi.org/10.1186/1559-0275-11-29

Neufeld, G., T. Cohen, S. Gengrinovitch, and Z. Poltorak. 1999. Vascular endothelial growth factor (VEGF) and its receptors. *FASEB J.* 13:9–22.

Nguyen, Q.D., D.M. Brown, D.M. Marcus, D.S. Boyer, S. Patel, L. Feiner, A. Gibson, J. Sy, A.C. Rundle, J.J. Hopkins, et al. RISE and RIDE Research Group. 2012. Ranibizumab for diabetic macular edema: results from 2 phase III randomized trials: RISE and RIDE. *Ophthalmology.* 119:789–801. http://dx.doi.org/10.1016/j.ophtha.2011.12.039

Oliver, J.A., and Q. Al-Awqati. 1998. An endothelial growth factor involved in rat renal development. *J. Clin. Invest.* 102:1208–1219. http://dx.doi.org/10.1172/JCI785

Ottiger, H.P., E.F. Battenberg, A.P. Tsou, F.E. Bloom, and J.G. Sutcliffe. 1990. 1B1075: a brain- and pituitary-specific mRNA that encodes a novel chromogranin/secretogranin-like component of intracellular vesicles. *J. Neurosci.* 10:3135–3147.

Pardoll, D.M. 2012. The blockade of immune checkpoints in cancer immunotherapy. *Nat. Rev. Cancer.* 12:252–264. http://dx.doi.org/10.1038/nrc3239

Peerschke, E.I., J.O. Minta, S.Z. Zhou, A. Bini, A. Gotlieb, R.W. Colman, and B. Ghebrehiwet. 2004. Expression of gC1q-R/p33 and its major ligands in human atherosclerotic lesions. *Mol. Immunol.* 41:759–766. http://dx.doi.org/10.1016/j.molimm.2004.04.020

Portela-Gomes, G.M., L. Grimelius, and M. Stridsberg. 2010. Secretogranin III in human neuroendocrine tumours: a comparative immunohistochemical study with chromogranins A and B and secretogranin II. *Regul. Pept.* 165:30–35. http://dx.doi.org/10.1016/j.regpep.2010.06.002

Ramos, J.W. 2008. The regulation of extracellular signal-regulated kinase (ERK) in mammalian cells. *Int. J. Biochem. Cell Biol.* 40:2707–2719. http://dx.doi.org/10.1016/j.biocel.2008.04.009

Rask-Madsen, C., and G.L. King. 2013. Vascular complications of diabetes: mechanisms of injury and protective factors. *Cell Metab.* 17:20–33. http://dx.doi.org/10.1016/j.cmet.2012.11.012

Robinson, C.J., and S.E. Stringer. 2001. The splice variants of vascular endothelial growth factor (VEGF) and their receptors. *J. Cell Sci.* 114:853–865.

Rong, Y.P., F. Liu, L.C. Zeng, W.J. Ma, D.Z. Wei, and Z.G. Han. 2002. Cloning and characterization of a novel human secretory protein: secretogranin III. *Sheng Wu Hua Xue Yu Sheng Wu Wu Li Xue Bao (Shanghai).* 34:411–417.

Scheppke, L., E. Aguilar, R.F. Gariano, R. Jacobson, J. Hood, J. Doukas, J. Cao, G. Noronha, S. Yee, S. Weis, et al. 2008. Retinal vascular permeability suppression by topical application of a novel VEGFR2/Src kinase inhibitor in mice and rabbits. *J. Clin. Invest.* 118:2337–2346. http://dx.doi.org/10.1172/JCI33361

Schwartz, S.G., H.W. Flynn Jr., and I.U. Scott. 2014. Emerging drugs for diabetic macular edema. *Expert Opin. Emerg. Drugs.* 19:397–405. http://dx.doi.org/10.1517/14728214.2014.938048

Shalaby, F., J. Rossant, T.P. Yamaguchi, M. Gertsenstein, X.F. Wu, M.L. Breitman, and A.C. Schuh. 1995. Failure of blood-island formation and vasculogenesis in Flk-1-deficient mice. *Nature.* 376:62–66. http://dx.doi.org/10.1038/376062a0

Sodhi, A., S. Montaner, and J.S. Gutkind. 2004. Viral hijacking of G-protein-coupled-receptor signalling networks. *Nat. Rev. Mol. Cell Biol.* 5:998–1012. http://dx.doi.org/10.1038/nrm1529

Stahl, A., K.M. Connor, P. Sapieha, J. Chen, R.J. Dennison, N.M. Krah, M.R. Seaward, K.L. Willett, C.M. Aderman, K.I. Guerin, et al. 2010. The mouse retina as an angiogenesis model. *Invest. Ophthalmol. Vis. Sci.* 51:2813–2826. http://dx.doi.org/10.1167/iovs.10-5176

Stefanini, M.O., F.T. Wu, F. Mac Gabhann, and A.S. Popel. 2009. The presence of VEGF receptors on the luminal surface of endothelial cells affects VEGF distribution and VEGF signaling. *PLOS Comput. Biol.* 5:e1000622. http://dx.doi.org/10.1371/journal.pcbi.1000622

Taupenot, L., K.L. Harper, and D.T. O'Connor. 2003. The chromogranin-secretogranin family. *N. Engl. J. Med.* 348:1134–1149. http://dx.doi.org/10.1056/NEJMra021405

Tokunaga, C.C., K.P. Mitton, W. Dailey, C. Massoll, K. Roumayah, E. Guzman, N. Tarabishy, M. Cheng, and K.A. Drenser. 2014. Effects of anti-VEGF treatment on the recovery of the developing retina following oxygen-induced retinopathy. *Invest. Ophthalmol. Vis. Sci.* 55:1884–1892. http://dx.doi.org/10.1167/iovs.13-13397

Valk, E., C.E. Rudd, and H. Schneider. 2008. CTLA-4 trafficking and surface expression. *Trends Immunol.* 29:272–279. http://dx.doi.org/10.1016/j.it.2008.02.011

van Dieren, S., J.W. Beulens, Y.T. van der Schouw, D.E. Grobbee, and B. Neal. 2010. The global burden of diabetes and its complications: an emerging pandemic. *Eur. J. Cardiovasc. Prev. Rehabil.* 17:S3–S8. http://dx.doi.org/10.1097/01.hjr.0000368191.86614.5a

Vasudev, N.S., and A.R. Reynolds. 2014. Anti-angiogenic therapy for cancer: current progress, unresolved questions and future directions. *Angiogenesis.* 17:471–494. http://dx.doi.org/10.1007/s10456-014-9420-y

Virgili, G., M. Parravano, F. Menchini, and J.R. Evans. 2014. Anti-vascular endothelial growth factor for diabetic macular oedema. *Cochrane Database Syst. Rev.* 10:CD007419. http://dx.doi.org/10.1002/14651858.CD007419.pub4

Wang, J., T. Takeuchi, S. Tanaka, S.K. Kubo, T. Kayo, D. Lu, K. Takata, A. Koizumi, and T. Izumi. 1999. A mutation in the insulin 2 gene induces diabetes with severe pancreatic β-cell dysfunction in the *Mody* mouse. *J. Clin. Invest.* 103:27–37. http://dx.doi.org/10.1172/JCI4431

Wang, Y., M. Cui, X. Cai, B. Sun, F. Liu, X. Zhang, and L. Ye. 2014. The oncoprotein HBXIP up-regulates SCG3 through modulating E2F1 and miR-509-3p in hepatoma cells. *Cancer Lett.* 352:169–178. http://dx.doi.org/10.1016/j.canlet.2014.05.007

Weissmiller, A.M., and C. Wu. 2012. Current advances in using neurotrophic factors to treat neurodegenerative disorders. *Transl. Neurodegener.* 1:14. http://dx.doi.org/10.1186/2047-9158-1-14

Wells, J.A., A.R. Glassman, A.R. Ayala, L.M. Jampol, L.P. Aiello, A.N. Antoszyk, B. Arnold-Bush, C.W. Baker, N.M. Bressler, D.J. Browning, et al. Diabetic Retinopathy Clinical Research Network. 2015. Aflibercept, bevacizumab, or ranibizumab for diabetic macular edema. *N. Engl. J. Med.* 372:1193–1203. http://dx.doi.org/10.1056/NEJMoa1414264

Yau, J.W., S.L. Rogers, R. Kawasaki, E.L. Lamoureux, J.W. Kowalski, T. Bek, S.J. Chen, J.M. Dekker, A. Fletcher, J. Grauslund, et al. Meta-Analysis for Eye Disease (META-EYE) Study Group. 2012. Global prevalence and major risk factors of diabetic retinopathy. *Diabetes Care.* 35:556–564. http://dx.doi.org/10.2337/dc11-1909

Zhong, Y., J. Li, Y. Chen, J.J. Wang, R. Ratan, and S.X. Zhang. 2012. Activation of endoplasmic reticulum stress by hyperglycemia is essential for Müller cell–derived inflammatory cytokine production in diabetes. *Diabetes.* 61:492–504. http://dx.doi.org/10.2337/db11-0315